Enhancing THz time-domain spectroscopy sensitivity using metamaterials and near-field approaches

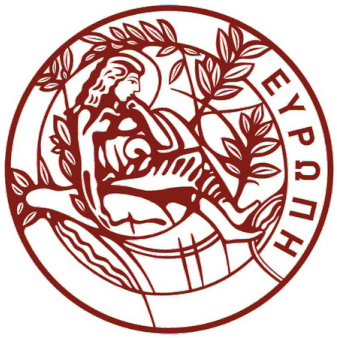

Constantinos Kerantzopoulos

Supervisor: Prof. Stelios Tzortzakis

Department of Physics
University of Crete

March 2023

Acknowledgements

I would like to thank my family for supporting me all these years even though they will not understand any of the contents of this work when I am going to explain it to them.

I want to thank Professor Stelios Tzortzakis for giving me a chance to become a part of this lab and for also giving me a second chance to remain a part of it. I want to thank Tasos Koulouklidis and Christina Daskalaki for guiding and helping me with this project, I would not have done it without you. Also, I would like to give my thanks to the rest of the team that helped me during my time here, Michalis Loulakis, Mary Manousidaki, Anna Tasolamprou, Ioannis Liontos, Apostolos Kyriakakis, Panagiotis Konstantakis, and Angeliki Sifaki.

Many thanks to my friends here in Herakleion who made my years in the university fun and unforgettable.

Abstract

Pesticides are widely used in agriculture to protect crops from pests and diseases, but their use can have harmful effects on human health and the environment. Pesticides can cause acute and chronic health effects, and they can also contaminate soil, water, and air. The detection of pesticide residues in food products is essential to ensure the safety and quality of the food supply. Food products are routinely tested for pesticide residues to ensure they comply with regulatory limits and are safe for human consumption.

In this work, we present a method for detecting pesticides in the THz region with the use of metamaterials. THz radiation has the potential to detect pesticides due to its ability to interact with molecular vibrations and rotational transitions in molecules, providing information on their chemical composition. The operating mechanism of the metamaterial is based on the concept of a change in the frequency at which it resonates. When the pesticide molecules come into contact with the metamaterial's surface, they change the refractive index of the surrounding medium, which causes a shift in the resonance frequency. Using THz spectroscopy, it is possible to detect and identify pesticides by measuring the shift in resonance frequency.

Due to a shortage of time, the data are preliminary, despite that, they show promise in the detection and identification of pesticides. Further research is needed to optimize the metamaterial-based sensor's performance and evaluate its performance under different experimental conditions.

Table of contents

1 Introduction **2**

1.1 The target of this project 2

1.2 Terahertz (THz) Radiation: Properties and applications 3

1.2.1 Properties of THz radiation 3

1.2.2 Applications of THz waves 4

1.3 Metamaterials 9

2 Experimental Techniques **11**

2.1 Generation of THz pulses with Photoconductive Antennas (PCAs) 11

2.2 Detection of THz pulses with Photoconductive Antennas (PCAs) 12

2.3 THz Time – Domain Spectroscopy (THz - TDS) 13

2.4 THz Near-Field and Far-Field Spectroscopy 17

2.4.1 Far-field THz-TDS system 18

2.4.2 Near-field THz-TDS system 19

3 Experimental Results **21**

3.1 Pesticides detection methods 21

3.1.1 Far - field results on fruit peels 22

3.1.2 Near - field results on fruit peels 26

3.1.3 Near - field results on thin films 27

3.2 Metamaterials assisted pesticide detection 29

3.2.1 Design and Simulations of metamaterials structures - Split Ring Resonators (SRRs) 29

3.2.2 SRRs created by Multi-photon polymerization (MPP) 29

3.2.3 SRRs designed by applying Babinet's principle 32

3.2.4 Asymmetric SRRs(aSRRs) designed by applying Babinet's principle 32

3.2.5 Active substances on SRRs in the far - field region 33

3.3 Conclusions and perspectives 41

4 Annex **42**
4.1 Fourier Transform Infrared Spectroscopy (FTIR) 42
4.1.1 FTIR results on fruit peels 43
4.2 Chiral metamaterials 46
4.3 Near - field Imaging 48
4.3.1 Calibration 48
4.3.2 Lighting 49
4.3.3 Resolution 50

References **52**

Chapter 1

Introduction

1.1 The target of this project

Food is a highly traded commodity worldwide, and as markets become increasingly globalized and the population continues to grow, the food supply chain becomes larger and more complex. This has led to a growing concern about food safety compliance and the presence of residues in food, prompting the need for new, rapid and non-destructive detection techniques that can be used for food quality evaluation and safety inspection. Terahertz Time Domain Spectroscopy (THz-TDS) is a promising technique for identifying unwanted chemical substances in food, such as pesticides.

Terahertz (THz) radiation interacts with polar molecules like water, but has weak interactions with non-polar molecules like plastics and ceramics, and is reflected by most metals. THz waves can penetrate typical packaging materials and textiles, allowing for detection of residues in food. Furthermore, different pesticides have distinct fingerprints in this frequency regime, allowing for separation from food powder matrices and other pesticides.

In this work, a number of pesticides with their respective active substances which are commonly used in agriculture, have been studied using THz-TDS in the THz range between 0.1 to 6 THz in the far-field region and between 0.1 to 3 THz in the near-field region. Also a different technique is used that utilizes metamaterials to enhance further the detection abilities of THz-TDS spectroscopy.

1.2 Terahertz (THz) Radiation: Properties and applications

1.2.1 Properties of THz radiation

The electromagnetic spectrum covers electromagnetic waves with frequencies ranging from Gamma rays to radio waves. The last years, one of the most interesting regions of the electromagnetic spectrum for exploring a number of scientific phenomena lies in the THz frequency range as it is shown in Fig. 1.1. THz radiation lies between the microwave and far infrared frequencies, from 0.1 THz to 30 THz. These frequencies correspond to a wavelength range from 3 mm to 10 μm, photon energy from 0.4 meV to 120 meV and to an equivalent black body radiation with temperatures between 4 K and 1200 K.

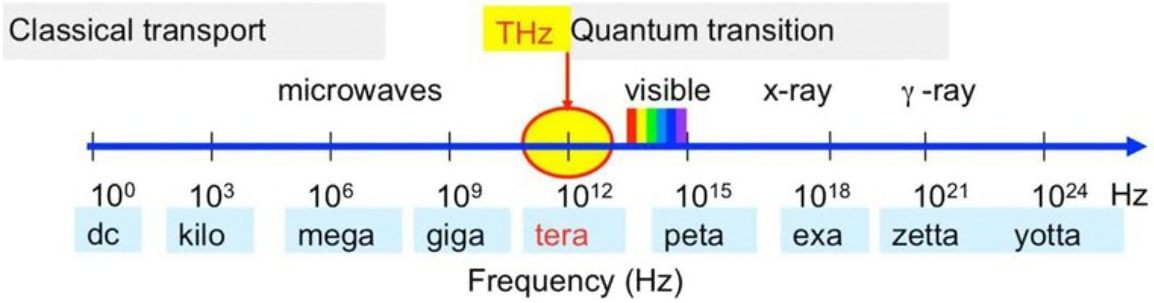

Fig. 1.1 Location of THz radiation in the electromagnetic spectrum.

Specifically, the frequency of 1 THz equals to a period of an electric field of 1 ps, a wavelength of 300 μm, a wavenumber of 33 cm^{-1}, an energy of 4.1 meV and a temperature of 47.6 K.

There are many THz sources, such as cosmic background radiation and black body radiation from objects at room temperature. Until recently the THz region was not particularly useful because there weren't good enough emitters to create a controlled signal nor sensors that had good efficiency for detection. Thus, the THz region was also known as the "THz Gap". A 1400 K black body source emits a few nWatts of power in the THz range onto a usual sample, while an oscillator produces power inversely proportional to frequency [1]. Many attempts from the electronic field from lower frequencies and the photonics field from higher frequencies were made to reach the THz frequencies. The first demonstration of a coherent emission and detection of broadband THz pulses in the late 1980's allowed to routinely access this part of the electromagnetic spectrum. Thus, the unique properties of THz radiation have been revealed, suggesting the development of promising applications [2].

First of all, THz waves have low photon energy (a few meV at 1 THz) and thus THz radiation can be used for many applications, such as biological, in a non-ionizing and non

destructive way. THz waves are safe for the samples and also for the operator due to the fact that they are heavily absorbed by water, this means that THz radiation cannot penetrate into the human body and can only cause minimal to no damage to the operator[3]. Furthermore, THz waves are less affected by Mie scattering and as a result, many dielectric materials, for example plastic, paper, wood and clothes are transparent to THz radiation. For this reason, they are used for non-destructive evaluation applications. Also, many molecules display strong absorption and dispersion due to rotational and vibrational transitions, unique for each molecule which allows spectroscopic fingerprinting in the THz region[4].

These characteristics make THz radiation applicable to many different fields. The applications of THz technology are divided into two parts, the THz imaging applications and the spectroscopic applications. Both of these categories have applications in medical science and biology, pharmaceutical and food industry , material science, art preservation, astronomy and security.

1.2.2 Applications of THz waves

In the field of medical science, THz radiation has the potential to aid in the detection of cancerous tissue in its early stages. This is because THz radiation can distinguish between healthy and cancerous cells based on differences in their dielectric properties[5]. In addition, THz imaging can be used to guide surgeons during cancer surgery. THz radiation can also be used in dental imaging to detect tooth decay and to image the internal structure of teeth, which could lead to better dental treatments[6]. Furthermore, THz radiation can aid in the detection and diagnosis of skin diseases such as melanoma, psoriasis, and eczema by analyzing the absorption spectra of the skin[7][8]. THz radiation also has been used in tomography as seen in Fig.1.2a.

Furthermore, THz radiation offers numerous applications in the field of biology because of its non-invasive and non-ionizing nature. Scientists have utilized THz radiation to study the structure and dynamics of biological macromolecules, such as proteins and DNA. THz spectroscopy can provide information about the intermolecular interactions, molecular vibrations, and energy levels of these molecules[9]. This information can be used to develop new drugs, gain insights into disease mechanisms, and design novel biomaterials. Additionally, THz radiation has been utilized to investigate the structure and function of cells. THz microscopy can provide high-resolution images of biological samples without damaging the sample. This technique has been used to study the morphology and behavior of cells, including cancer cells. Moreover, THz radiation can be used to identify and classify microorganisms based on their unique THz spectra. This technique has been used to detect and identify bacteria, viruses, and other microorganisms[10].

The pharmaceutical industry can benefit from THz radiation for studying the molecular structure of pharmaceutical compounds. THz radiation can provide information about the chemical composition, crystal structure, and the presence of impurities in these compounds, which is crucial for drug discovery and quality control. Furthermore, THz radiation can be utilized to investigate the interaction between drugs and excipients, enabling the development of better drug formulations. THz radiation can also be used to monitor the quality of pharmaceutical products during manufacturing, as seen in Fig.1.2b, as it can detect changes in the THz spectrum of the drug that may indicate changes in its chemical composition or crystal structure. Additionally, THz radiation can aid in the detection of counterfeit drugs, as each drug has a unique THz spectrum. If the spectrum of a drug does not match the known spectrum, it may be a fake[11][12].

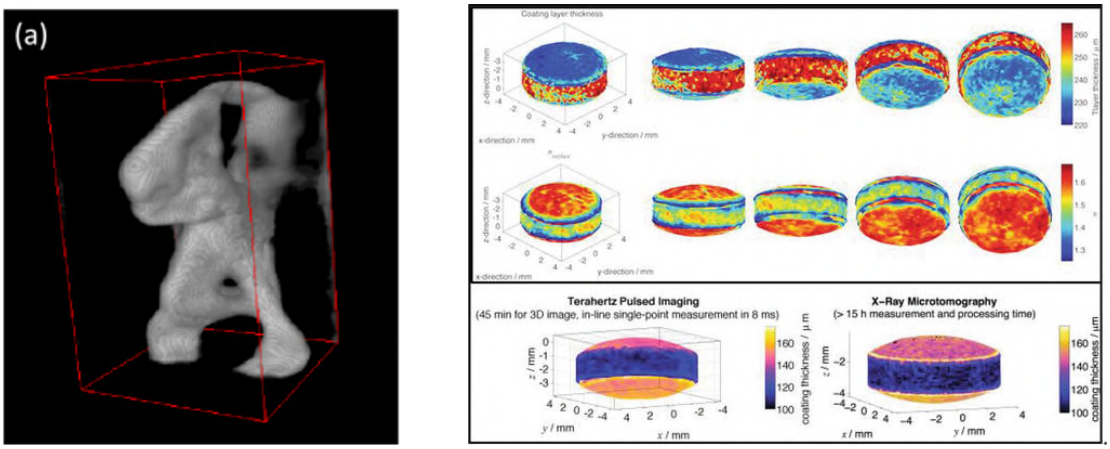

(a) (b)

Fig. 1.2 Tomography of a bone with THz(a) and quality control in the pharmaceutical industry(b).

Moreover, THz imaging can be applied in the food industry as a quality control tool to detect defects, such as cracks or voids, in food products such as fruits, vegetables, and baked goods. Additionally, THz spectroscopy can be used to measure the water content and other properties of food products. THz radiation can also be utilized to identify foreign objects, such as metal or plastic, in food products, as well as to detect and quantify contaminants such as bacteria, fungi(see Fig.1.3), or pesticides. THz spectroscopy can be used to monitor different stages of food processing, such as drying, baking, and cooking. It can also be used to monitor the ripeness and quality of fruits and vegetables during storage and transportation[13][14][15].

THz radiation has also various applications in material science, where it can be used to non-destructively investigate the physical and chemical properties of materials[16]. THz

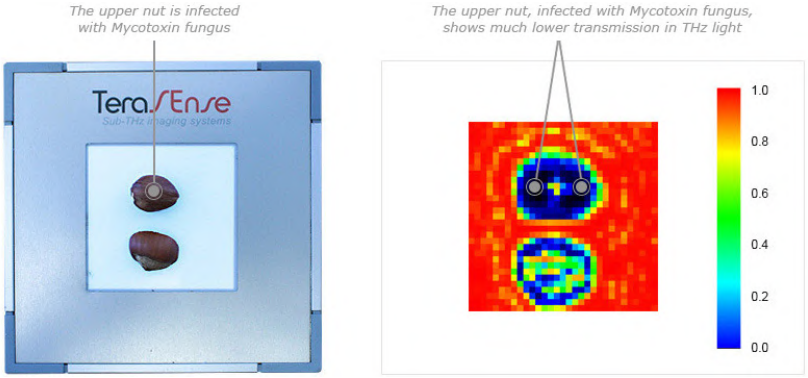

Fig. 1.3 Detection of fungi during food quality control.

spectroscopy, for instance, can be utilized to explore the dynamics of molecular vibrations in materials, thereby providing insights into their chemical composition and molecular structure. THz imaging can be used for quality control in manufacturing processes, such as detecting defects in semiconductors or monitoring the thickness of coatings. THz radiation can also be used for non-destructive testing of materials, such as identifying cracks and defects in structures like pipes or bridges. Furthermore, THz radiation can be used to study the structural integrity of composite materials, like those used in aerospace applications[17]. The emerging field of Terahertz plasmonics combines the unique properties of THz radiation with metallic nanostructures to develop new materials and devices with tunable THz responses. THz plasmonics can be applied to develop highly sensitive sensors for detecting small amounts of chemicals, as well as high-speed switches and modulators for THz communication[18].

In art conservation, THz radiation is used to study the materials in art objects. THz imaging is particularly useful for investigating the inner layers of paintings to understand the techniques used by the artist, the artwork's condition, and any changes that may have occurred over time as seen in Fig.1.4. One of the benefits of using THz radiation is that it's non-invasive, which means that artwork doesn't need to be physically altered or disturbed for analysis. This is crucial for delicate and valuable works of art. THz radiation is used to analyze materials used in art, like pigments, varnishes, and adhesives, to understand their chemical composition and develop conservation strategies. THz imaging can also detect hidden or obscured layers in artwork, like underdrawings, providing insight into the artist's creative process. THz radiation has enormous potential in art preservation and conservation, making it a valuable tool for researchers and conservators in this field[19][20].

THz radiation plays a crucial role in various astronomical applications, particularly in the exploration of the early universe and in the detection of molecules in space. The analysis of the Cosmic Microwave Background(CMB), which is the residual radiation from the Big Bang, can be significantly improved by utilizing THz radiation. Specifically, the THz band offers

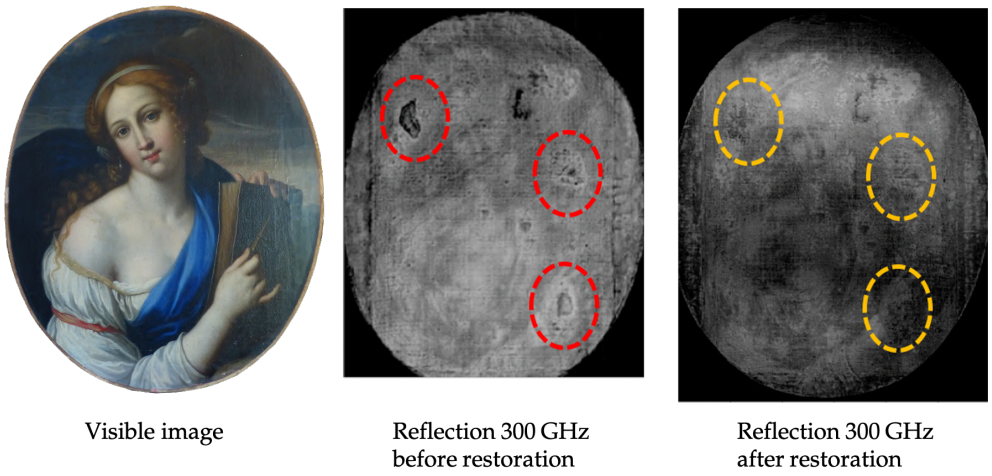

Fig. 1.4 Detection of defects in painting during restoration process.

valuable insight into the polarization of the CMB, which provides fundamental understanding of the early universe and the nature of dark matter. The detection of numerous molecules in space is made possible by the spectral lines found within the THz range. Consequently, THz astronomy serves as an essential tool for identifying these molecules. For instance, THz radiation has been employed to detect various molecules, including water vapor, carbon monoxide, and others, in the interstellar medium[21]. Furthermore, THz radiation enables the examination of the initial stages of planet and star formation. As an example, THz telescopes are utilized to investigate protoplanetary disks, which are the disks consisting of gas and dust surrounding young stars that eventually coalesce into planets. Additionally, THz radiation has significant implications in the study of black holes[22].

In the security field, THz imaging technology has been studied for use in security screening, particularly in detecting concealed weapons or explosives on individuals or in baggage. THz radiation is also able to penetrate through clothing and other materials that would typically obstruct visible light, making it useful in detecting hidden objects as seen in Fig.1.5. One advantage of THz radiation is that it is non-ionizing, meaning it does not carry enough energy to cause ionization or damage to cells and tissues. This makes it safer for use in security screening than X-rays, which carry a higher risk of radiation exposure. In addition to screening for concealed objects, THz radiation can also be used in spectroscopic analysis to detect and identify chemicals and materials. THz spectroscopy has been studied for use in identifying hazardous chemicals or explosives in the field[23], characterization of substances based on their spectra is presented in Fig.1.5b

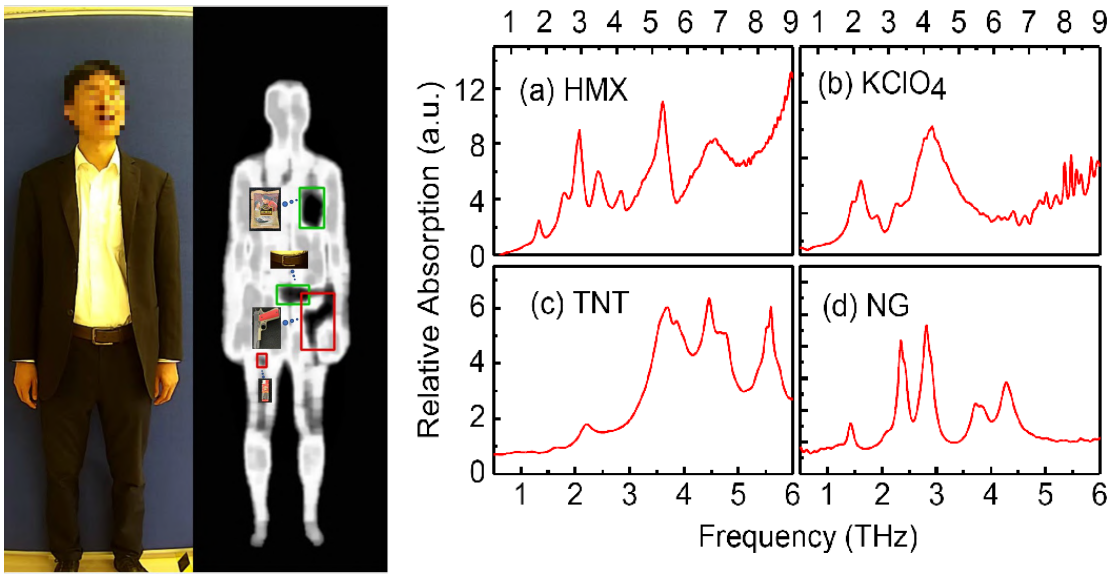

(a) (b)

Fig. 1.5 Application of THz in security as weapon detector and in the characterization of unknown substances.

1.3 Metamaterials

Metamaterials are an array of artificially made metallic structures of sub-wavelength dimensions that gain their properties from the geometry of the structures rather than the materials that consist them. These sub-wavelength structures enable the material to affect the electromagnetic waves differently than the usual bulk materials. The subwavelength structures in metamaterials are usually designed to have specific geometries and properties that give rise to novel electromagnetic properties, such as negative refractive index[24][25], negative relative permittivity or negative relative permeability, chirality as seen in section 4.2, cloaking, and superlensing. Thus far, they can be found being used in a large region of the electromagnetic spectrum containing far - IR, mid - IR, near - IR and optical frequencies[26] [27][28]. The basic unit of a metamaterial is known as a meta-atom, which is typically much smaller than the wavelength of the electromagnetic wave being manipulated. The arrangement of meta-atoms in a metamaterial is what gives it its unique electromagnetic properties. The electromagnetic properties of a metamaterial can be controlled by adjusting the size, shape, orientation, and spacing of the meta-atoms, as well as the materials they are made of.

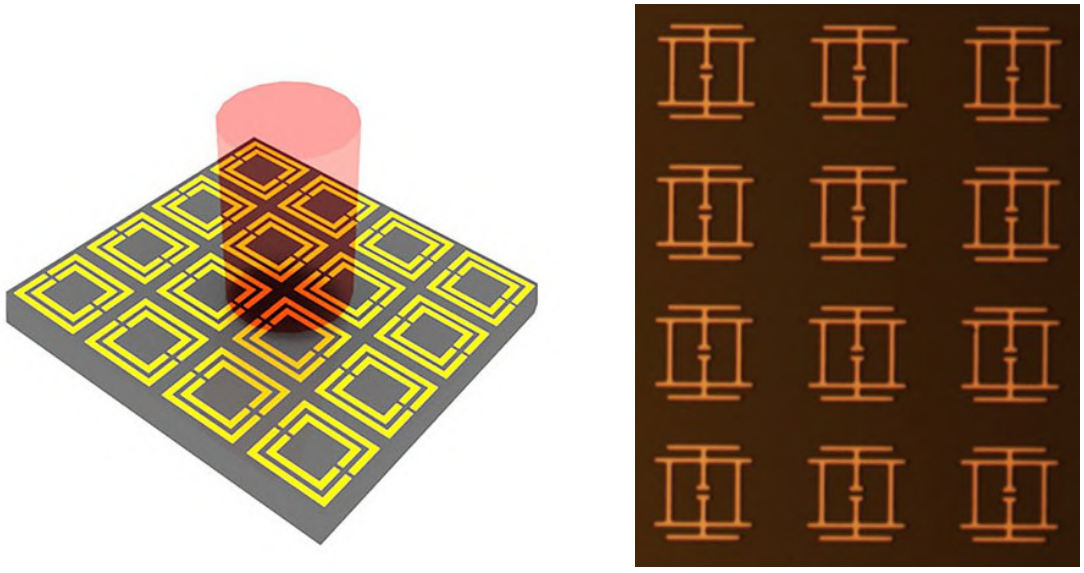

(a) (b)

Fig. 1.6 Different designs of metamaterial structures.

Metamaterials have a wide range of potential applications in various fields such as communications, aerospace and defense, imaging, solar energy, and medical applications. In communications, they can be used to improve the performance of antennas by designing them to operate more efficiently with higher gain and directivity. In aerospace and defense, metamaterials can be used for stealth technology, radar systems, and components such as

filters and antennas. They can also be used to create superlenses for high-resolution microscopy, medical imaging, and nanolithography. In solar energy, metamaterials can improve the efficiency of solar cells by enhancing light absorption. Lastly, in medical applications, metamaterials can be used for drug delivery and tissue engineering by creating nanostructures and scaffolds to target specific cells and support new tissue growth. [29]

One application of metamaterials in detection is in the area of biosensing. Biosensors are devices that detect and measure biological molecules, such as proteins or DNA, and are used in a variety of applications including medical diagnosis, environmental monitoring, and food safety. Metamaterials can be designed to have a specific response to certain biological molecules, allowing them to be used as sensors. For example, a metamaterial-based biosensor might be designed to change its refractive index or absorption properties in response to the presence of a specific biomolecule, which can be detected and measured.

Similarly, metamaterials can be engineered to interact with chemical substances in a specific way, enabling their detection and identification for chemical detection purposes. There are different mechanisms by which metamaterials can detect chemicals, such as changes in the electromagnetic properties of the metamaterial when a chemical is present, or changes in the resonant frequency of the metamaterial due to chemical binding.

One approach for chemical detection using metamaterials in the THz range is to use them as part of a THz spectroscopy system. Metamaterials can be used to create THz absorbers and filters that selectively absorb or transmit THz radiation at specific frequencies, which enables the detection and identification of chemicals. With this method several papers have been written in the detection and identification of pesticides. More specifically, Lee et al. have developed a near-field method of detecting pesticides in concentrations ranging from 10^4-10^6ppb via the use of a nano-antenna metamaterial[30]. While Chen et al. and Qu et al. are able to detect even lower concentrations in the range of 0.01 to 0.5 ppb with the use of a metamaterial absorbers[31][32].

Chapter 2

Experimental Techniques

2.1 Generation of THz pulses with Photoconductive Antennas (PCAs)

Photoconductive antennas (PCAs) are one of the most popular methods for generating THz pulses. In the late 1980s, THz pioneers David Auston and Daniel Grischkowsky's research groups were able to emit and detect pulsed broadband THz radiation from optically pumped PCAs [33]. As shown in Fig. 2.1, a PCA consists of two metallic electrodes on a semiconductor substrate, typically a low-temperature grown III-V semiconductor like GaAs. In order for a THz pulse to be generated, the PCA is illuminated with a femtosecond laser pulse with photon energies higher than the semiconductor's bandgap, generating photo-induced free carriers. By applying a bias voltage between the electrodes, these carriers are accelerated across the gap by the bias field, resulting in a current and producing THz radiation. Due to the pulsed nature of the laser beam, the current's amplitude is a function of time, and the derivative of the current with respect to time generates the THz pulse. The resulting THz wave is polarized perpendicular to the bias field and in the same direction as the space between the electrodes. The derivative of the current with respect to time is the THz electric field.

$$J(t) \propto E_{bias} N(t) \tag{2.1}$$

$$E_{THz} \propto \frac{\partial J(t)}{\partial t} \tag{2.2}$$

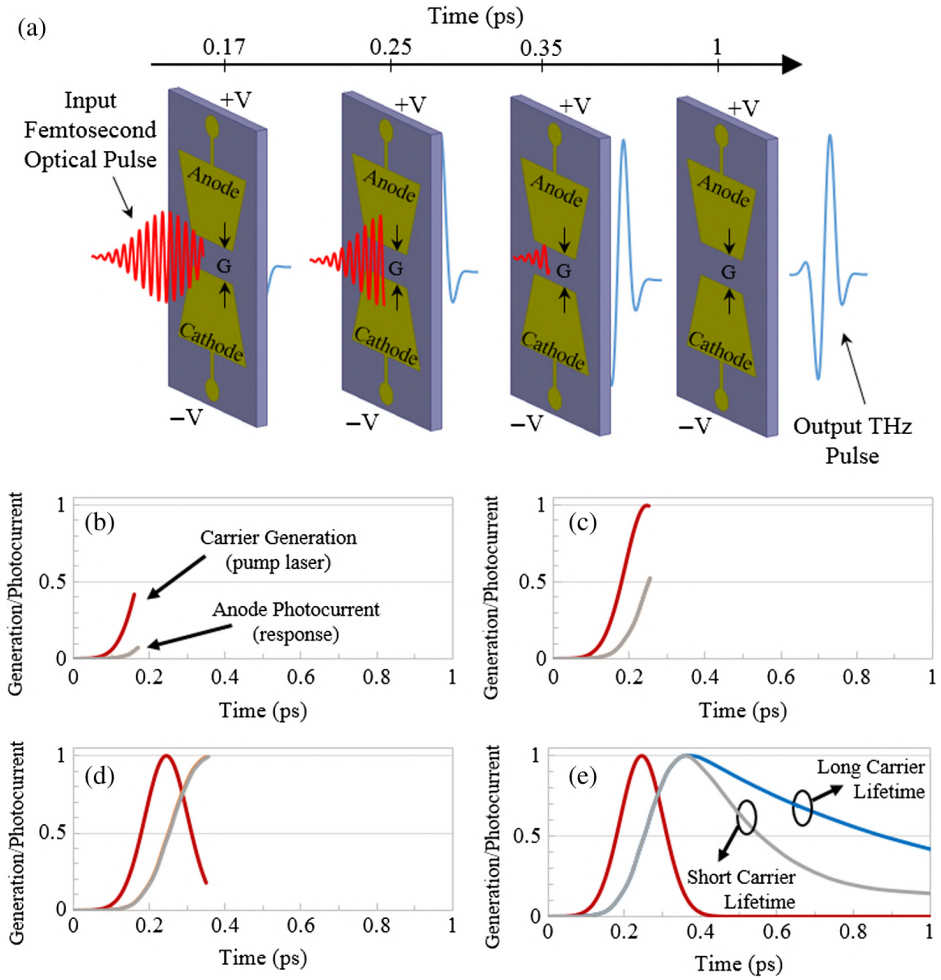

Fig. 2.1 Illustrative example of pulsed THz generation in a PCA. (a) A femtosecond optical pulse illuminates the PCA, generates a transient photocurrent, which drives the antenna, and is re-emitted as a broadband THz pulse. (b–e) Time profile of the carrier generation (red trace) and photocurrent in the antenna gap for photoconductive material (gray trace) for short-carrier lifetime and (blue trace) for long carrier lifetime. Image taken from [33]

2.2 Detection of THz pulses with Photoconductive Antennas (PCAs)

The configuration of a PCA utilized as a detection device is closely comparable to that of a PCA used for emission. To operate a PCA as a detector, the photo-current produced by the probe beam across the gap between the electrodes is measured while biased by the THz electric field as shown in Fig. 2.2. This current is then collected and measured. If no electric field is applied across the gap, the probe beam's photo-carriers diffuse randomly and do not create any net current. Conversely, when the gap is illuminated by a THz wave, the electric

field associated with the wave separates the electron-hole pairs, generating a net current. This transient current is proportional to the applied THz electric field.

$$J(t) \propto E_{THz}N(t) \tag{2.3}$$

PCAs designed for detection generally have much narrower gaps, typically around 10 micrometers, compared to PCAs used for emission, which have gaps of over 50 micrometers. This is because narrower gaps require less electric field to bias the structure and produce a measurable current [34].

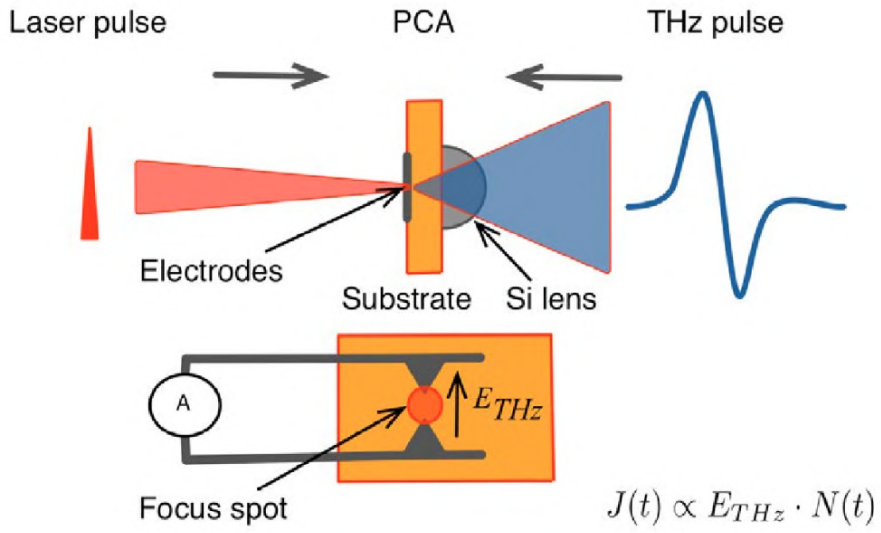

Fig. 2.2 Illustrative example of pulsed THz detection in a PCA

2.3 THz Time – Domain Spectroscopy (THz - TDS)

In the previous two sections, we have been introduced to the classic approaches for the emission and detection of THz radiation. Here, the basic requirements in order to build a THz time-domain spectrometer (THz-TDS) are presented. Our THz-TDS system is based on a pump-probe, coherent detection approach. A laser beam generated by a laser source is split into two arms, the pump beam and the probe beam. Those two pulses have a defined temporal relationship. The pump beam is used to generate THz pulses in a PCA and interacts with the sample, while the probe beam is used to pump the PCA responsible for the detection of the THz pulse. The probe beam propagates along a delay line and then interacts with the THz beam, thus giving information for the electric field of the THz pulse in relation to

time. A representation of this procedure is in Fig. 2.3. A more detailed description of the experimental setup will be presented in the next sections.

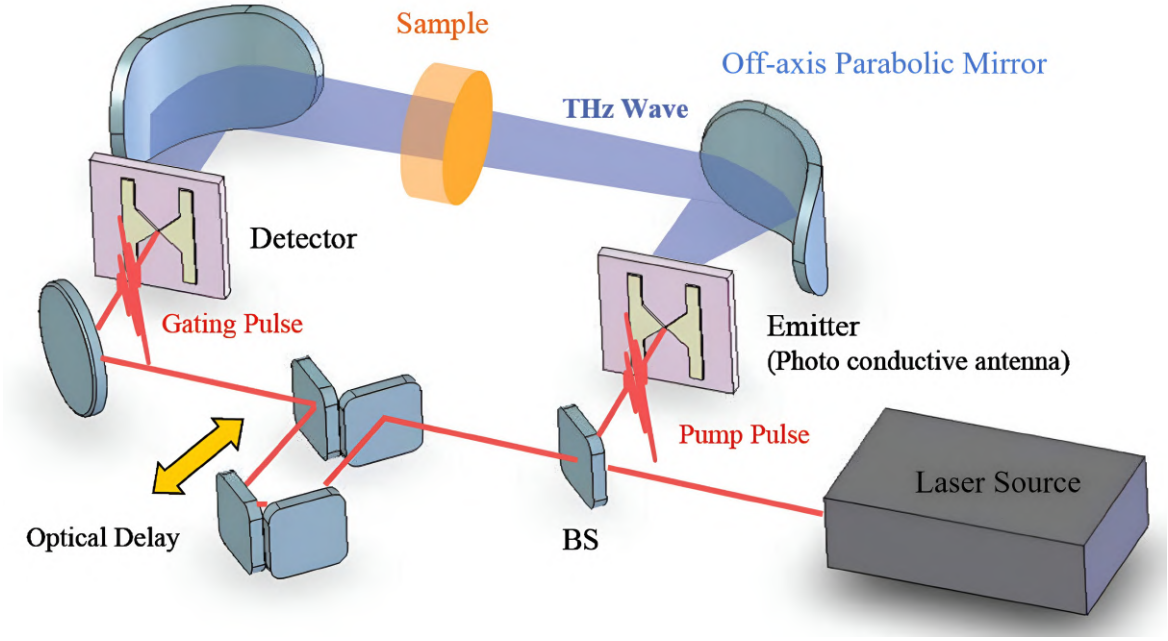

Fig. 2.3 Schematic of a THz Time-Domain Spectroscopy system.

A very useful and unique characteristic of THz time-domain spectroscopy is that it provides information on the amplitude and phase of the electric field. Taking the Fourier transform of the THz electric field, we can extract this information in the frequency domain.

$$E(\omega) = A(\omega)e^{-i\Phi(\omega)} = \int E(t)e^{-i\omega t}dt \tag{2.4}$$

The transformation of the electric field into the frequency domain by FFT is displayed in Fig. 2.4

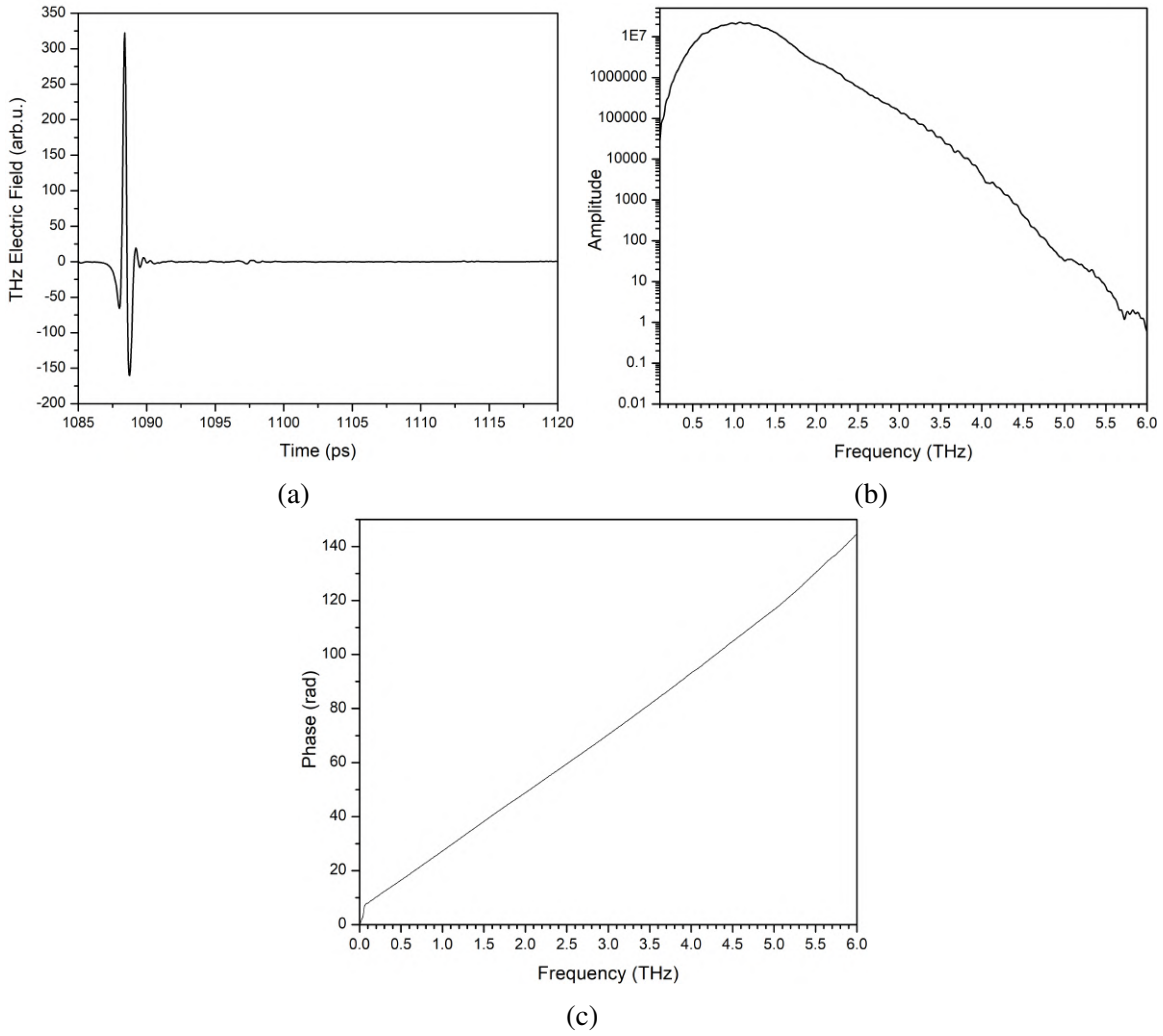

Fig. 2.4 The recorded Electric field of the THz pulse(a), the pulse's spectral amplitude(b) and the phase of the electric field(c).

In THz-TDS, the THz beam interacts with the sample and undergoes changes depending on the optical, chemical and structural properties of the sample are under investigation. In general, there are three main physical effects to be taken into account in the measurement process; absorption, transmission, and scattering. Absorption is the energy transfer from the THz wave to certain modes of the sample. In general, the intensity of a light beam propagating through a material obeys the Beer-Lambert law:

$$I = I_0 e^{-\alpha d} \tag{2.5}$$

where I_0 is the intensity of the beam prior to propagation through a material of thickness d and absorption coefficient α.

The knowledge of the amplitude and the phase of the electric field enables the study of absorption and dispersion spectroscopy. Knowing that the reference electric field, E_{ref}, is given by the equation $E_{ref} = A_R(\omega)e^{-i\Phi_R(\omega)}$ and that the field of the pulse that interacts with the sample, E_{sam}, is $E_{sam} = A_S(\omega)e^{-i\Phi_S(\omega)}$ we can calculate the following quantities[35].

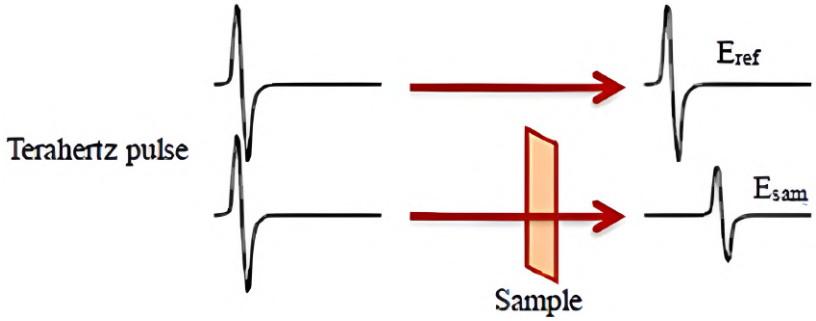

Fig. 2.5 Schematic of a THz Time-Domain Spectroscopy system.

The refractive index can be described as:

$$n = 1 + \frac{[\Phi_S(\omega) - \Phi_R(\omega)]}{\omega d}c \tag{2.6}$$

where Φ_S is the phase of the electric pulse of the sample, Φ_R is the phase of the electric pulse of the reference, ω is the angular frequency, d is the sample thickness and c is the speed of light.

The absorption coefficient can derived by the equation:

$$\alpha = -\frac{2}{d}\ln\left(\frac{A_S(\omega)}{A_R(\omega)}T\right) \tag{2.7}$$

where d is the sample thickness, A_S is the amplitude of the sample spectrum, A_R is the amplitude of the reference spectrum and T is the Fresnel reflection coefficient for normal incidence, and it is given by $T = \frac{(n(\omega)+1)^2}{4n(\omega)}$.

The complex permittivity can be calculated from the refractive index:

$$\varepsilon^{'} = n^2 - k^2 \tag{2.8}$$

$$\varepsilon^{''} = 2nk \tag{2.9}$$

where n is the real part of the refractive index and k is the extinction coefficient given by $k = \frac{\lambda\alpha}{4\pi} = \frac{c\alpha}{2\omega}$.

The absorbance is given by the following equation:

$$A(\omega) = -ln(\frac{A_S(\omega)}{A_R(\omega)}) \tag{2.10}$$

2.4 THz Near-Field and Far-Field Spectroscopy

THz near-field and far-field spectroscopy are two complementary techniques used to study materials at THz frequencies. Near-field THz spectroscopy refers to the detection and analysis of THz fields that are generated close to the sample surface, typically within a distance of less than one wavelength from the source, and is classified into two groups: the reactive near-field and the radiating near-field (also known as the Fresnel region). In the near-field, charges and currents generate a localized area where the electromagnetic field exhibits different behavior than electromagnetic radiation. The charges in this area create electric dipoles, and the currents generate magnetic ones. These fields have a fixed phase relationship with each other and together constitute the near-field. In the reactive near-field area, both the strength of the electric field (E) and the magnetic field (H) can be independently measured [36].

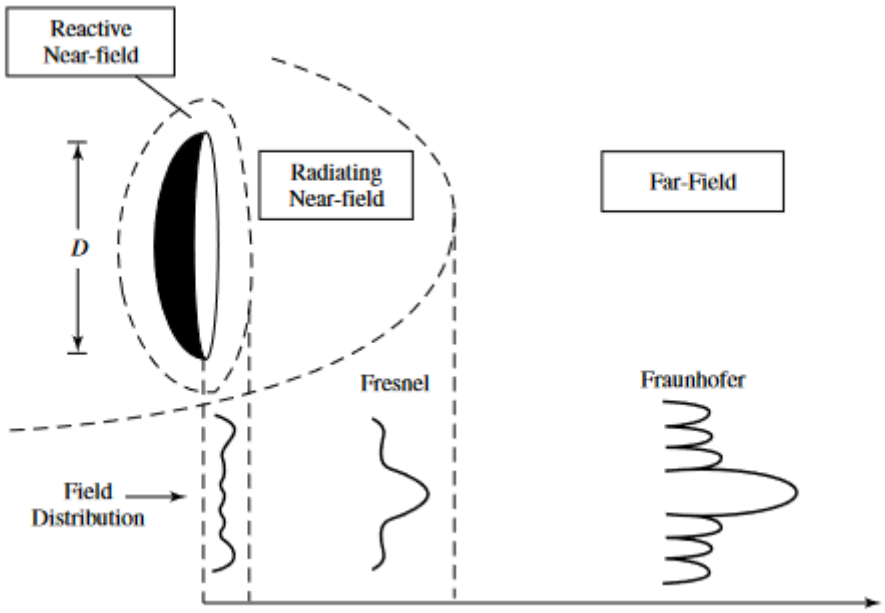

Fig. 2.6 Change of the amplitude pattern shape as it moves away from the antenna.

The radiating near-field, which is located between the reactive near-field and the far-field region, exhibits characteristics of both its surrounding regions. In this zone the radiating field dominates, and the angular field distribution depends on from the distance from the source. The energy of the fields in the near-field region decreases according to the inverse cube law due to their dipole nature, this is the reason the near-field is detectable in distances really close to the sample. The near-field technique enables high spatial resolution measurements and has the ability to distinguish subwavelength features of the sample. This method is particularly useful for studying materials with unique surface properties or geometries, including thin films, biological cells, and nanomaterials.

On the other hand, far-field or Fraunhofer THz spectroscopy refers to the detection and analysis of THz radiation that has propagated to a distance from the source that is greater than one wavelength. The far-field technique is more commonly used and involves detecting the electromagnetic radiation that has been transmitted, reflected or diffracted by the sample. Far-field THz spectroscopy is a non-destructive method for probing the properties of materials in the THz range. It is particularly useful for studying bulk materials, where the transmitted THz waves reveal the absorption and reflection properties of the material. Far-field THz spectroscopy is also capable of probing the electronic and vibrational properties of materials, including the presence of impurities, defects, and other structural features, making it an essential tool for materials science and physics research. All the above zones can be seen in Fig.2.6, they have no sudden changes at their boundaries and are simply divided in order to characterize the fields easier[37].

For the needs of this thesis, THz spectroscopic measurements both in the far-field and the near-field are needed, and thus two different experimental setups were used and are presented in the following sections.

2.4.1 Far-field THz-TDS system

For the far-field studies, a typical THz-TDS system was used based on photoconductive antennas (TOPTICA TeraFlash pro). A laser system that can deliver 80 fs pulses centered at 1560 nm with a repetition rate of 100 MHz was used. The laser pulses were guided through a set of fibers on the PCA antennas, where THz pulses with a spectral content in the range of 0.1 to 6 THz were generated. A schematic representation of the experimental setup can be seen in Fig. 2.7. After the THz pulse is produced by the PCA emitter, it was guided and focused through two parabolic mirrors, on the surface of a mechanical stage where the sample is placed. The beam can then either be reflected by or transmitted through the sample, operating this way in reflection or in transmission mode respectively. In both geometries, the reflected or transmitted beam is guided through another pair of parabolic mirrors to the PCA

detector. An optical imaging system consisting of a camera, a mirror, and a lens was utilized for the proper and precise placement of the sample at the correct position.

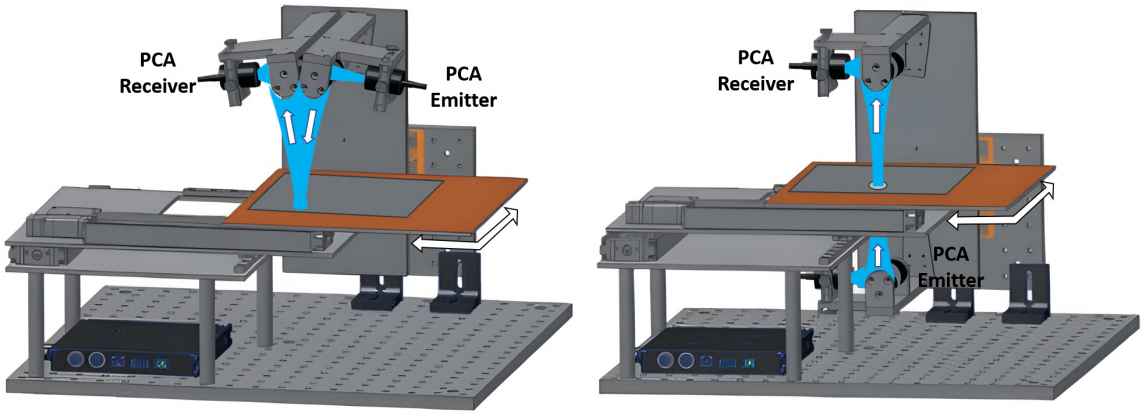

Fig. 2.7 Far-field setup for Reflectance measurements (left) and for Transmittance measurements (right).

2.4.2 Near-field THz-TDS system

In order to study samples in the near-field zone, an appropriate experimental setup was developed that operated only in transmission mode. In detail, the generation part of the setup remained the same with the one utilized for the far field measurements. However, for the detection of the THz waves a near-field THz detector (see Fig.2.8) was purchased (Protemics). A detailed view of the experimental setup is depicted in Fig2.4.2. Practically, this near-field detector operates under the same principles as the PCAs. The only difference is that the gap between the electrodes is very close to the edge of the tip, allowing this way for the detection of THz waves at a very close proximity ($\approx 20\mu m$) to the studied sample. To excite the semiconductor between the two electrodes, a femtosecond laser pulse at 780 nm was used, provided by frequency doubling the 1560 nm beam of the main laser system through a second harmonic module. Since the signal received by the micro-probe is rather weak, it goes through an amplifier that raises the signal by six to eight orders of magnitude. A 3D-axis motorized stage was used in order to properly place the sample under the tip.

The setup also contains two optical imaging systems. The first one consists of a camera and microscope objective lens and it is placed right next to the micro-probe. With that system, we can see the surface of the sample at approximately twenty times magnification. In order to monitor the position and the distance of the micro-probe above the sample, a second imaging system consisting of a camera and a lens was used. This system was placed diagonally to the sample and roughly at the same height as the stage.

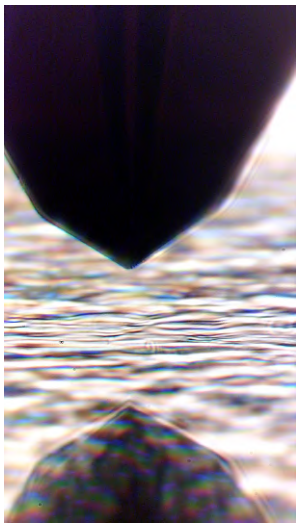

Fig. 2.8 Image of the THz micro-probe.

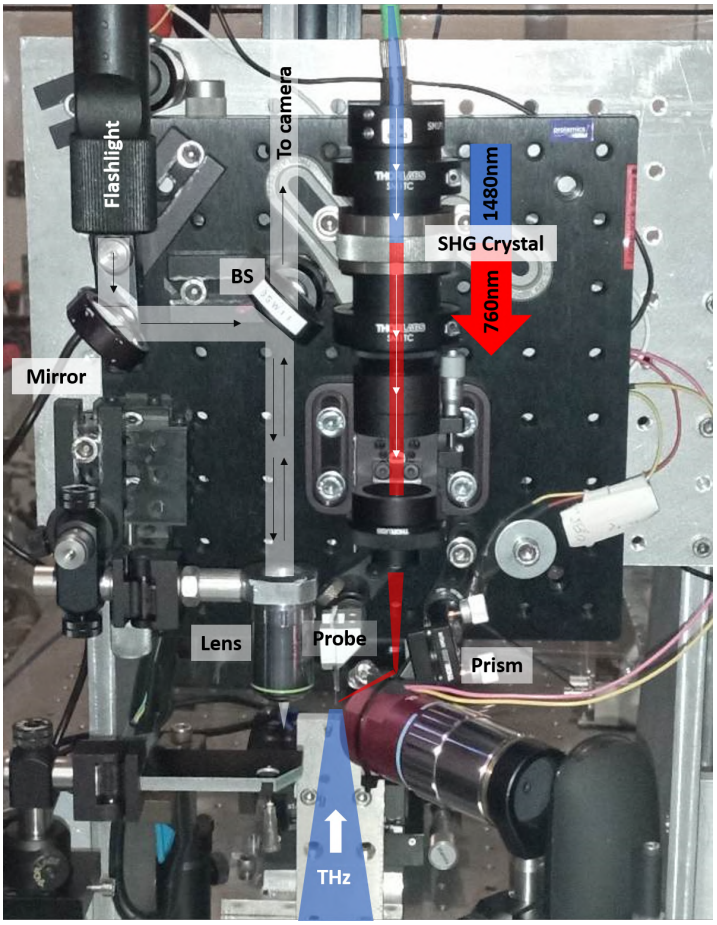

Fig. 2.9 Image of the near-field system, with the path of the laser beams on top.

Chapter 3

Experimental Results

3.1 Pesticides detection methods

An accurate detection method helps with the monitoring of the amount of pesticides used by farmers in agriculture. The concentrations used should be below the maximum allowed limits that are set by the proper health-safety authorities, for example in Fig.3.1 are presented various fruits and vegetables with the corresponding maximum amount concentration of pesticide allowed. High-performance liquid chromatography, mass spectroscopy, and gas chromatography are methods used heavily in the last years to detect pesticides. The THz radiation has only started being applied in the detection of pesticides but only at an experimental level. As mentioned before many molecules present distinct transitions in the THz region, so it is only logical to focus on this region for the creation of a method that would help in their detection and identification. Also, by being non- ionizing radiation, a nondestructive technique may be developed.

We begin our measurements with the simplest method that may yield any results, by performing THz spectroscopy in the far-field region in fruit and vegetable peels covered in pesticide.

Fruits and Vegetables	Metalaxyl (ppb)	Acetamiprid (ppb)	Abamectin (ppb)	Imazalil (ppb)	Phosmet (ppb)
Apples	1000	400	30	10	500
Oranges	700	900	40	4000	500
Avocados	10	10	10	10	50
Potatoes	20	10	10	10	50
Tomatoes	300	500	90	300	50
Cucumbers	500	300	40	500	50

Fig. 3.1 Table of the maximum allowed concentration in ppb of various active substances of pesticides by the European Commission.

3.1.1 Far - field results on fruit peels

To detect pesticides, we started by applying them to fruit and vegetable peels. The fruit and vegetable peels were made the day before the measurements and were left to dry to become dehydrated because any amount of water contained in them can heavily absorb THz and would affect our measurements. We used apple and cucumber peels for the project. The pesticide we used is ProfilExtra, acquired by the lab, and its active substance is Acetamiprid. More active substances will be used in this project so a list of the various pesticides available and their active substances is presented in Fig. 3.2.

Plant protection products (Pesticides, Insecticides)	Active substance
Affirm	Emamectin benzoate
Voliam Targo	Chlorantraniliprole + Abamectin
Profil Extra 5SL	Acetamiprid
Altacor 35WG	Chlorantraniliprole
Assist	Cypermethrin
Vylathrin 10EW	a-Cypermethrin
Karate 10CS	λ-Cyhalothrin
Phosmetar 50WP	Phosmet
Insignia 20W	Pyraclostrobin
Aliette	Fosetyl-Al
Doble	Abamectin
Roundup	Glyphosate
Ridomil Gold	Metalaxyl + Mancozeb
LBG-01F34	Potassium phosphonates
Scomrid aerosol	Imazalil
-	Thiabendazole
-	Phosphonic acid
Rogor	Dimethoate
Dursban	Chlorpyrifos
Mesurol	Methiocarb

Fig. 3.2 Table of various Pesticides and their respective active substances.

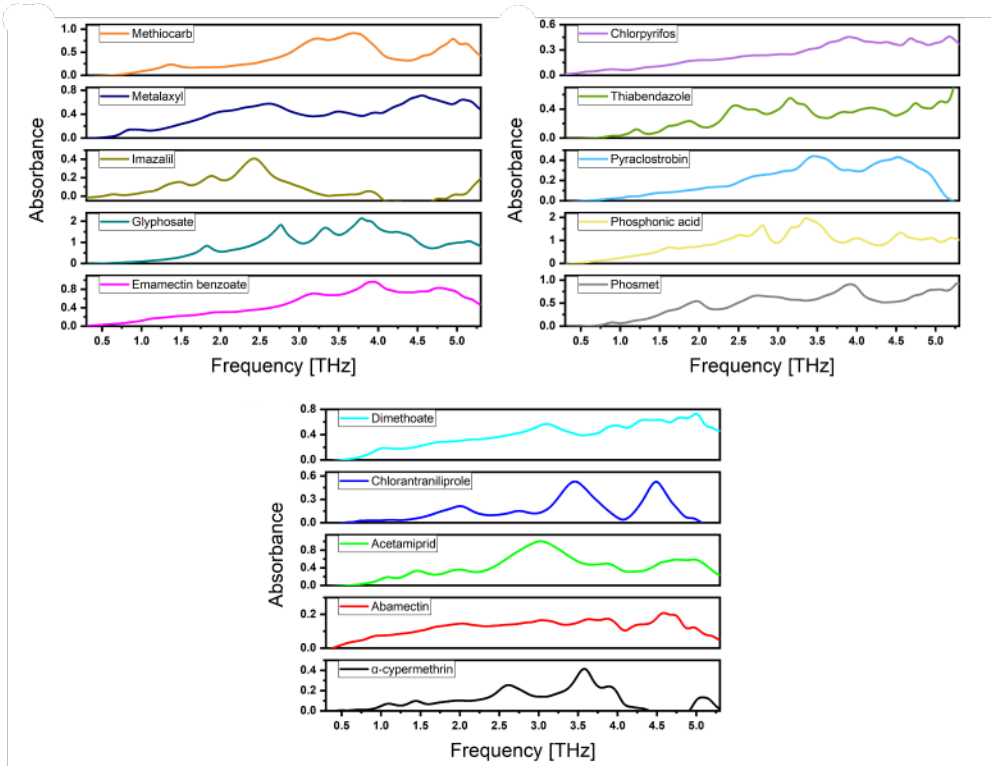

Fig. 3.3 Absorbance spectra of active substances in the THz region. The figures contain Methiocarb, Metalaxyl, Imazalil, Glyphosate, and Emamectin Benzoate(top left), Chlorpyrifos, Thiabendazole, Pyraclostrobin, Phosphonic acid, and Phosmet(top right), Dimethoate, Chlorantraniliprole, Acetamiprid, Abamectin, and α-cypermethrin(bottom).

ProfilExtra was diluted in water to create different concentrations of samples, the minimum amount of these samples were used to cover the surface of the cucumber and apple peels and then they were left again to dry, for about an hour, before getting measured. Some of the peels we prepared can be seen in Fig. 3.4 The peels were measured in the THz far-field system in reflection mode. We specifically chose ProfilExtra because its active substance, Acetamiprid, has a peak around 1.4 THz so it may be visible in the spectra of the cucumber and apple peels. The absorbance spectra of Acetamiprid and other active substances that exist in the lab can be seen in Fig. 3.3. We proceed to measure the fruit peels of cucumber and apple on the far-field THz system in reflection, the measurements are presented in Fig. 3.5.

Fig. 3.4 Image of the cucumber peels used in the project.

The peak that we hoped to see at 1.4 THz from the active substance of ProfilExtra is not visible in any of the samples. Also, we did not observe a clear relationship between the reflection and the concentration of ProfilExtra, for example, higher overall absorption in the samples with more pesticide, this may be due to the non-flat surface of the samples. These measurements were made in the reflection mode of the setup and as such the reflected THz wave becomes too random from the non-flat surface of the fruit and we cannot extract any information from the measured absorption. With these data, we are not even able to say with confidence whether the surface is covered in pesticide or not, for this reason, we need a new method.

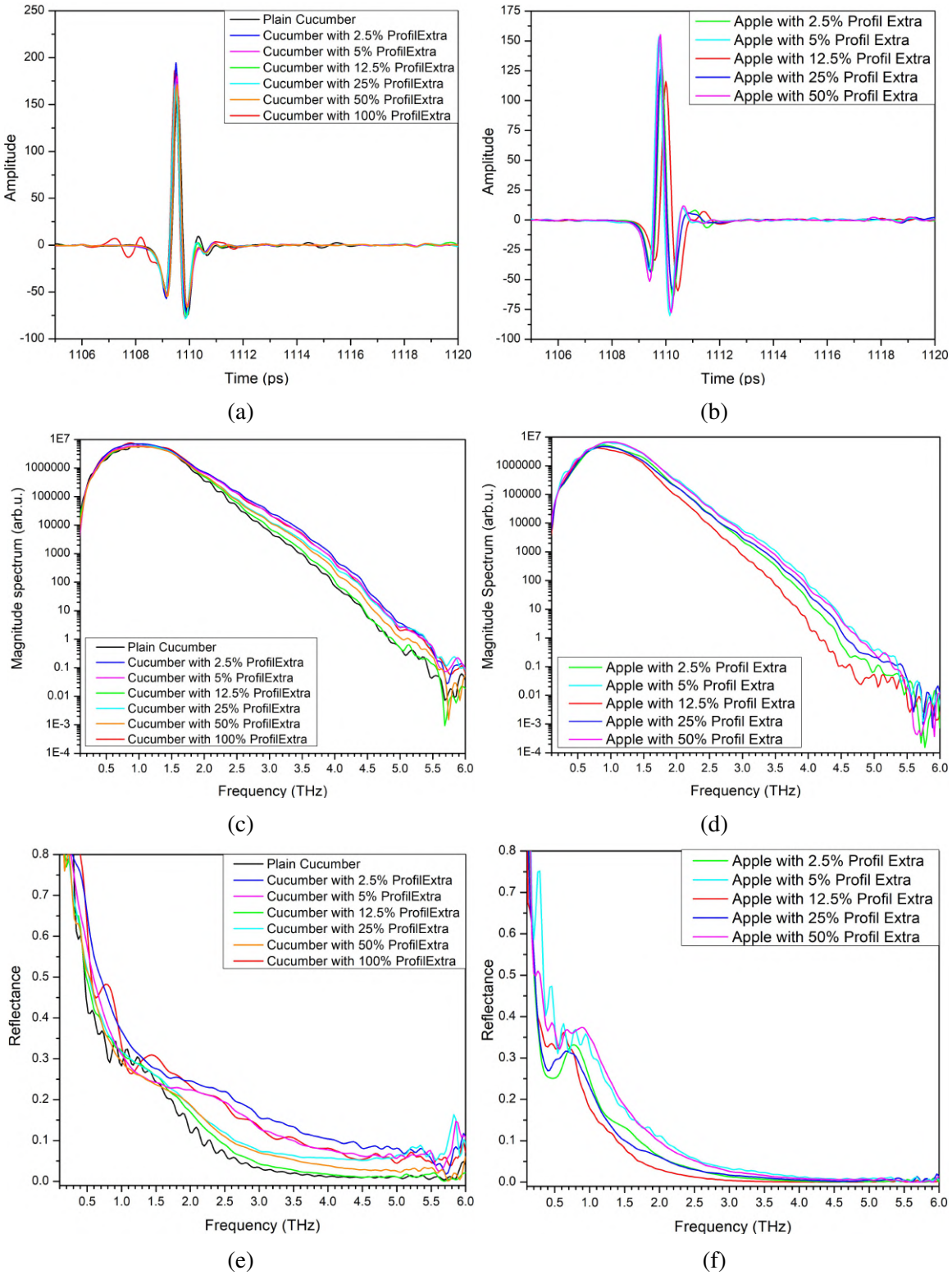

Fig. 3.5 Measured amplitude of the electric field(a)(b), magnitude spectrum(c)(d) and reflectance(e)(f) of cucumber and apple peels. The data for the cucumber peels are (a)(c)(e) and for the apple peels (b)(d)(f).

3.1.2 Near - field results on fruit peels

We were not able to detect ProfilExtra in the far-field region so our next step is to repeat the measurements in the near-field system. The measurements will be done in transmission because the near-field system can only measure in this mode. With the same method as before we created only apple peels covered in ProfilExtra. This time we made two concentrations to cover the apple peels with, 50% and 100%. We measured multiple areas of the apple peel surface with 100% ProfilExtra, an apple peel with 50% ProfilExtra, and a plain apple peel at the THz near-field system. The data are presented in Fig. 3.6.

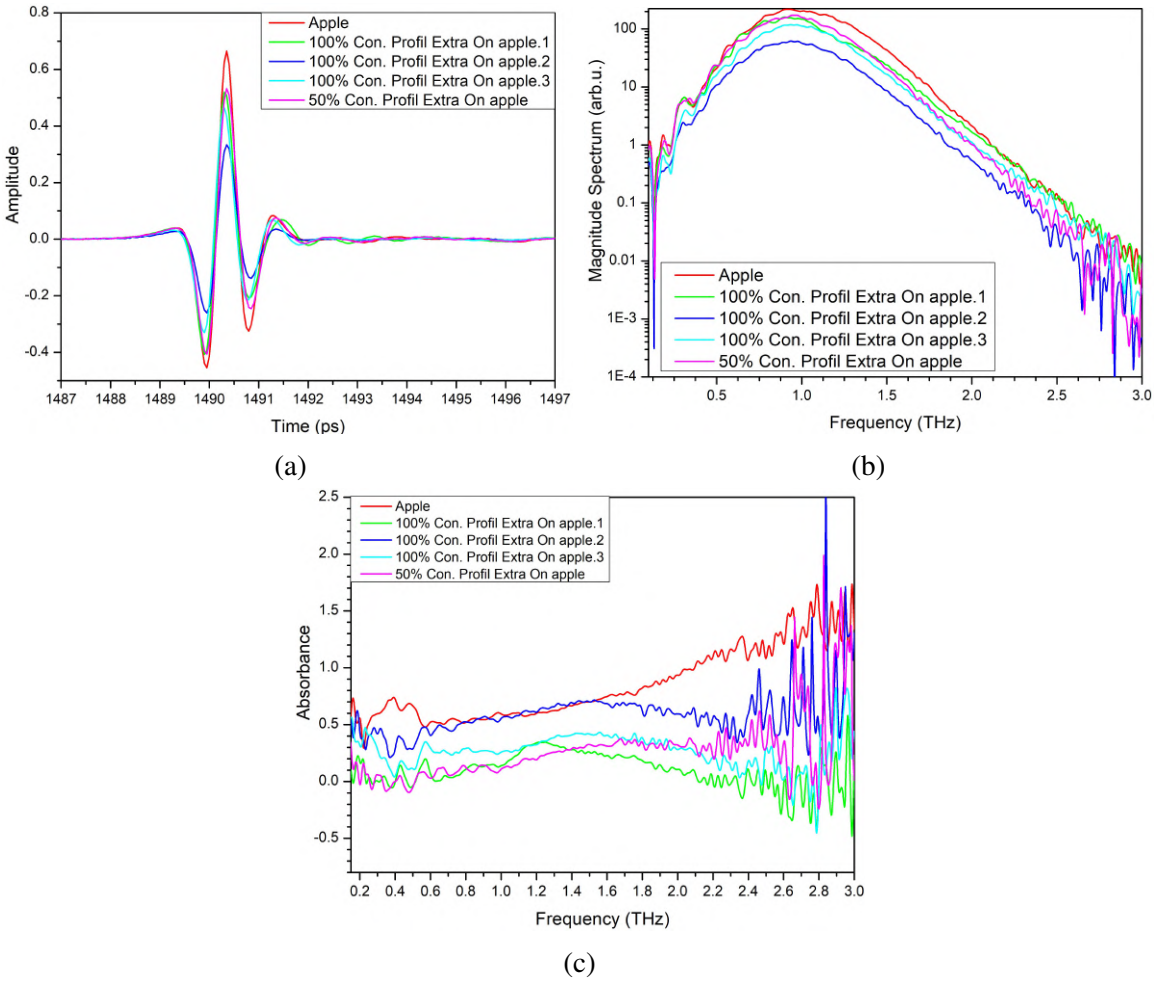

(a) (b)

(c)

Fig. 3.6 Measured amplitude of electric field(a), magnitude spectrum(b) and absorbance(c) of different concentrations of ProfilExtra on apple peels. The numbering in the 100% ProfilExtra measurements corresponds to different areas of the same sample.

We received the same inconclusive results as before. The peak of Acetamiprid at 1.4 THz is not visible in any of the samples, this method did not yield results due to the randomness

of the sample's surface or due to the low signal, or perhaps due to our inexperience with the near-field system at the time.

3.1.3 Near - field results on thin films

To eliminate the randomness of the fruit's surface we stopped using apple peels as samples, instead, we replaced them with nylon films. By stretching the films over a ring in order to have an even surface we remove the random factor the non-flat surface imposed, also nylon is transparent in the THz region and as a result, we measure a higher signal. We applied pure ProfilExtra to the surface of the films. The measurements that are presented in Fig. 3.7 were made around the same sample-tip distance of 45um.

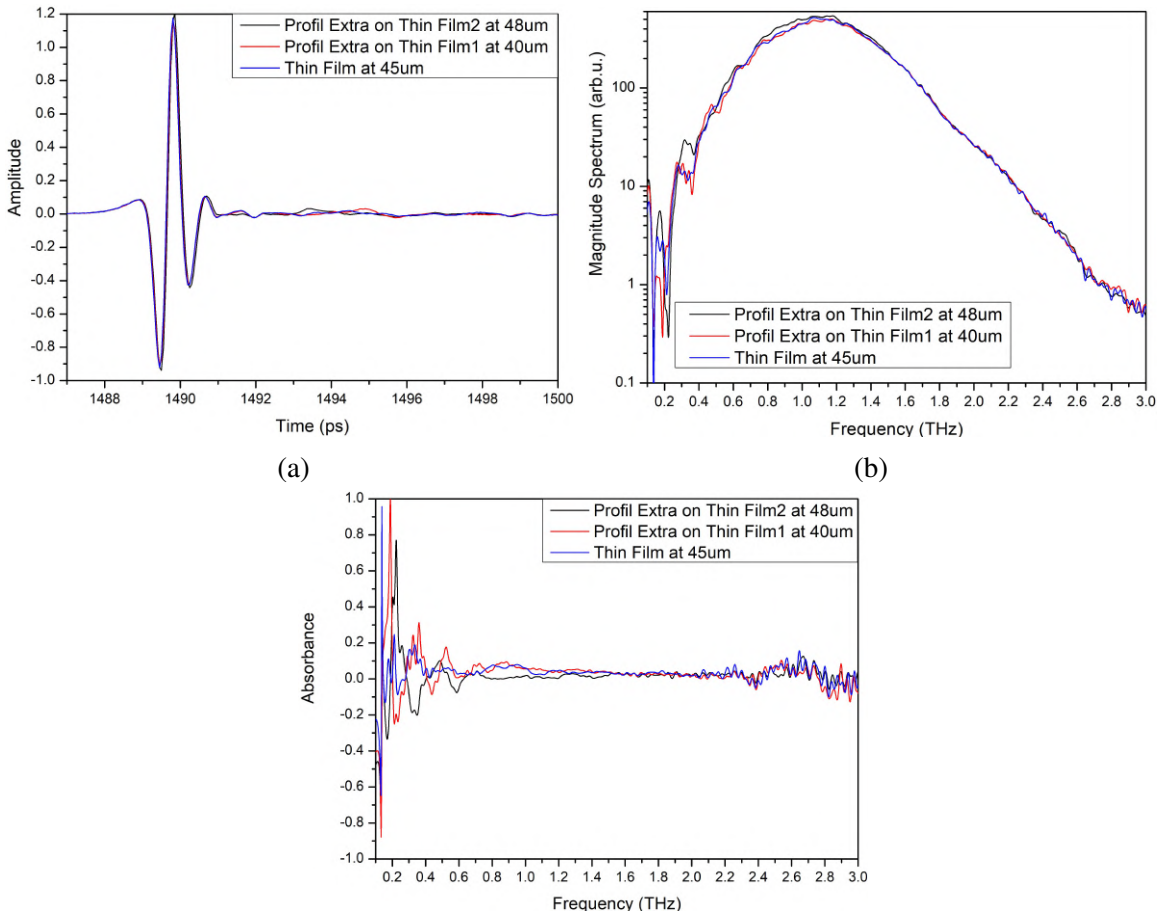

Fig. 3.7 Amplitude of the electric field(a), magnitude spectrum, and absorbance of three thin films accompanied with their respective distance from the micro-probe. Two of the thin films were covered in ProfilExtra and one was plain.

We can observe that the films covered in ProfilExtra and the plain one have similar spectra. Although we used pure ProfilExtra the near-field system does not have enough sensitivity to detect the one drop that we applied to each film. None of these methods proved successful in the detection of ProfilExtra. It is clear at this point that simple THz spectroscopy cannot detect even the highest concentration of pesticide due to the little amount of substance deposited on the samples. We need a new method to be able to detect small amounts of substances. The combination of metamaterials and THz radiation may be the solution. Simple THz spectroscopy is not sufficient by itself to detect small amounts of substances but with the help of the proper metamaterial to act as a sensor we may be able to reach really low concentrations.

3.2 Metamaterials assisted pesticide detection

3.2.1 Design and Simulations of metamaterials structures - Split Ring Resonators (SRRs)

The metamaterial structure we are using for the detection of the active substances is called Split Ring Resonator or SRR. These structures exhibit resonance at a specific frequency that depends on the dimensions of the structure. The idea behind this method is to use various SRRs to create multiple resonances. By studying the shift of the resonances in relation to different concentrations and different pesticides deposited on the surface of the metamaterial a way may be found to map out the behavior of the shifts, the basic principle of the experiment is depicted in Fig 3.8. Three different types of SRRs were used, SRRs created by Multi-photon polymerization(MPP), SRRs created by Babinet's principle, and asymmetric SRRs created by Babinet's principle. The SRRs created by MPP operate in transmission, while the ones created by Babinet's principle operate in reflection. The structures were designed and simulated in the software called Comsol.

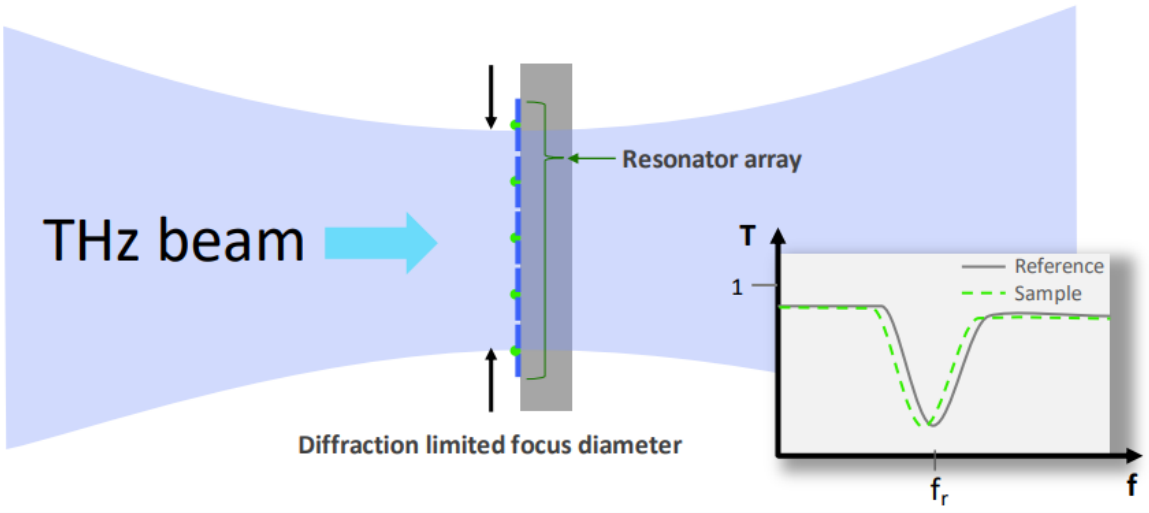

Fig. 3.8 The principle of our experiment.

3.2.2 SRRs created by Multi-photon polymerization (MPP)

These SRRs are metallic structures made of silver and deposited in a Silicon substrate. They were made by polymerizing a photopolymerizable resin with a tightly focused ultrashort laser pulse on a Silicon substrate. After the desired structure was formed, the remaining resin was washed away by an alcohol[38]. The whole structure is coated with silver by selective

electroless silver plating[39]. The dimensions of the structures were chosen so the SRR exhibits resonance in 0.5 THz and 1 THz at x polarization, simulations of the reflectance and transmittance are presented in Fig 3.9, also other variations were designed but ended up not being used are in Fig 3.11. The SRRs were scanned in SEM, and images of them are presented in Fig 3.10.

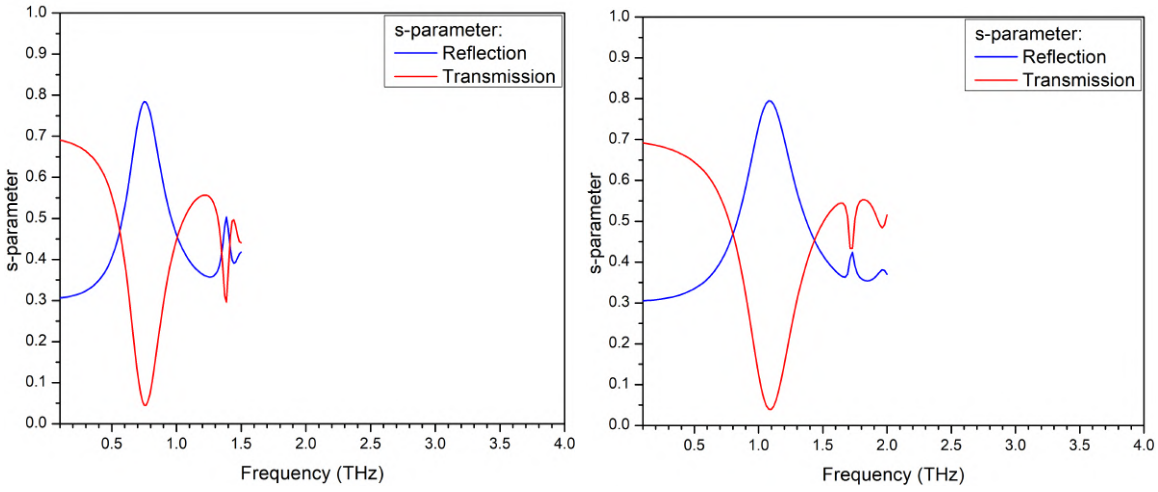

(a) (b)

Fig. 3.9 Simulated Reflection and Transmission spectra of the SRRs at x polarization. (a) are the spectra for the SRR designed to exhibit resonance around 0.5THz and (b) are the spectra for the design of 1 THz.

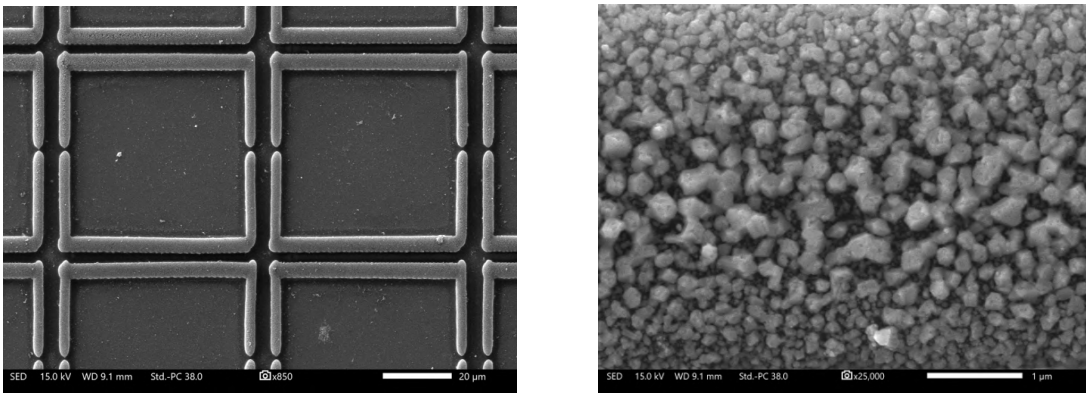

(a) (b)

Fig. 3.10 SEM images of the SRRs produced by MPP at x850 (a) and x25000 (b). In the second image we can easily see the porosity of the silver particles created by the metallization process.

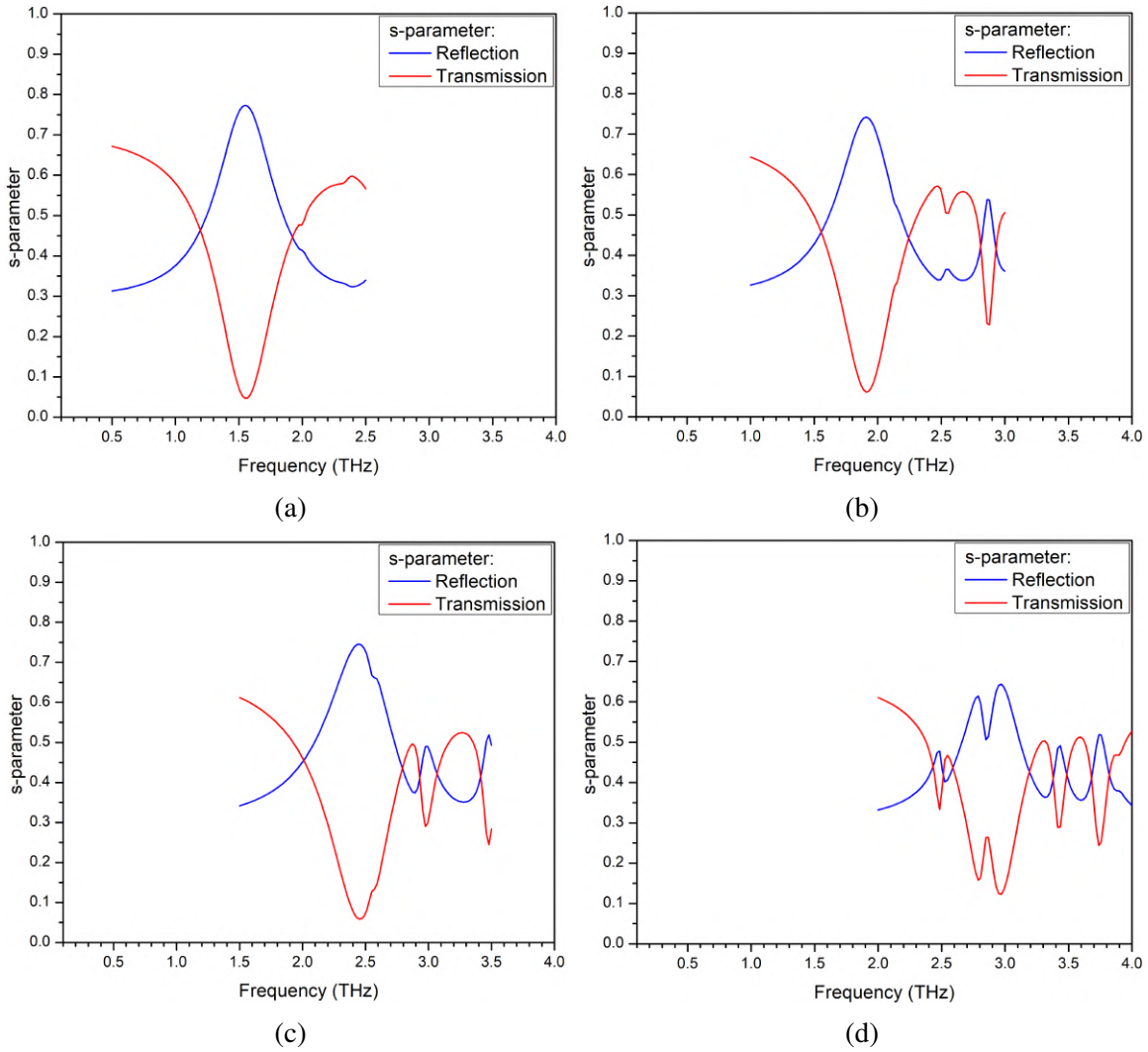

Fig. 3.11 Spectra of various other SRR designs for this project. They exhibit resonance at 1.6(a), 2(b), 2.5(c), 3(d).

3.2.3 SRRs designed by applying Babinet's principle

As can be seen from Fig.3.10, the MPP technique results in metallic structures with porous surface. Such samples are not easy to be cleaned between consequent measurements. In order to overcome this issue, an alternative fabrication method was adopted, that of carving with the laser beam the desired design on top of a gold substrate. Such SSR structures follow the Babinet's principle, meaning that the shape of the structure is not built on top but carved out of the metal. The metamaterial was fabricated by gold spattering a glass substrate and then removing the gold with laser ablation to carve out the proper design. After that, the sample was washed with an alcohol to remove excess gold particles displaced by the laser ablation process[40]. SEM images of these SRRs are presented in Fig 3.12

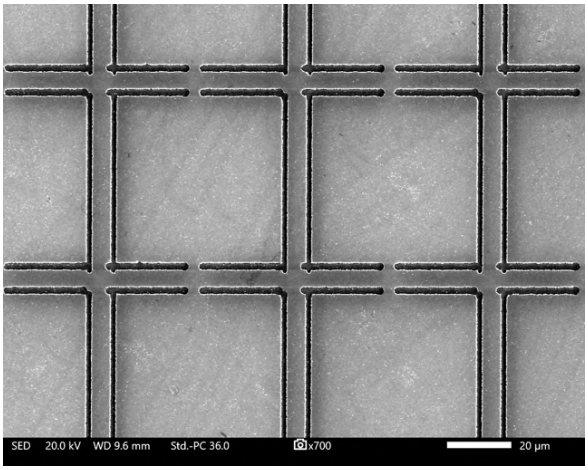

Fig. 3.12 SEM image of the Babinet's SRRs at x700

3.2.4 Asymmetric SRRs(aSRRs) designed by applying Babinet's principle

In order to achieve sharp resonances, the previously symmetric design of the SSR structures, was modified with an asymmetric one. Such asymmetric SRRs have the potential to result in significantly sharper resonances, enabling this way more precise measurements. The asymmetric SRRs were constructed by the same method as the previous SRRs, but they have different geometry. This time the gap the structures have is not in the middle but shifted by a few micrometers, this asymmetry offers sharper resonances and a different shape than before. The design of the aSRRs and their simulated function are displayed in Fig 3.13a.

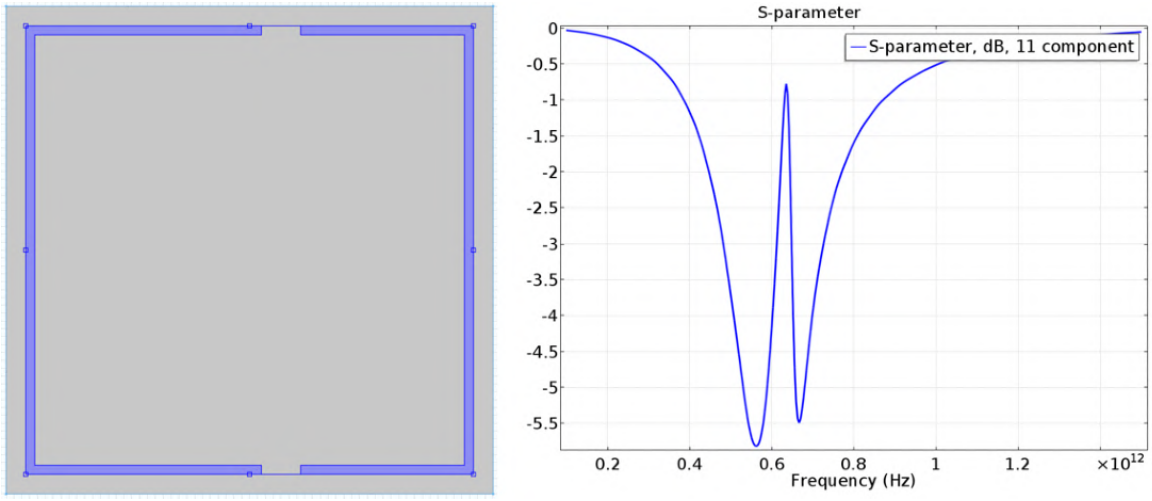

(a)

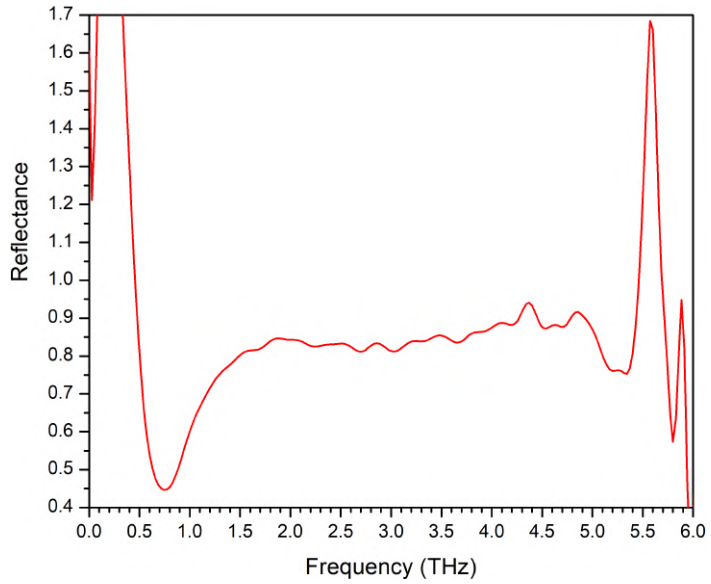

(b)

Fig. 3.13 Design of a single unit of the aSRRs (left) and the simulated function of the metamaterial(right)(a) and the experimental data of the same structure(b).

3.2.5 Active substances on SRRs in the far - field region

In our measurements, we decided to start by using only the active substances of pesticides and not pesticides themselves. The active substances were diluted in distilled water or ethanol, depending on the metamaterial used.

At the SRRs created by MPP, we noticed that there is a shift in the resonance when a drop of water is deposited onto the metamaterial. If a second drop is added, the resonance stays at the same frequency as it was with the one drop. So, the first drop of water causes a

shift, and then the rest drops do not cause any more shifts. If we use ethanol, we notice again a shift at the first drop. The second drop of ethanol causes also a shift and the third drop and so on. Ethanol somehow affects the metamaterial, so we decided to use distilled water as our diluent in the metamaterials made by MPP.

At the SRRs constructed by Babinet's principle, water causes the same changes as it did to the SRRs made by MPP. Ethanol does not affect the metamaterial this time and acts in the same way as water, so at these metamaterials, we use ethanol as our diluent because it dries faster than water to save time.

SRRs created by MPP

We prepared samples of several different concentrations of active substances diluted in distilled water. The active substances we used were Acetamiprid and Metalaxyl and the concentrations of these samples ranged from 10 ppb to 10^5 ppb. We chose Acetamiprid and Metalaxyl due to the position of their absorption peaks in their spectra, which is around 1 THz, similar to the frequency of the metamaterials resonance.

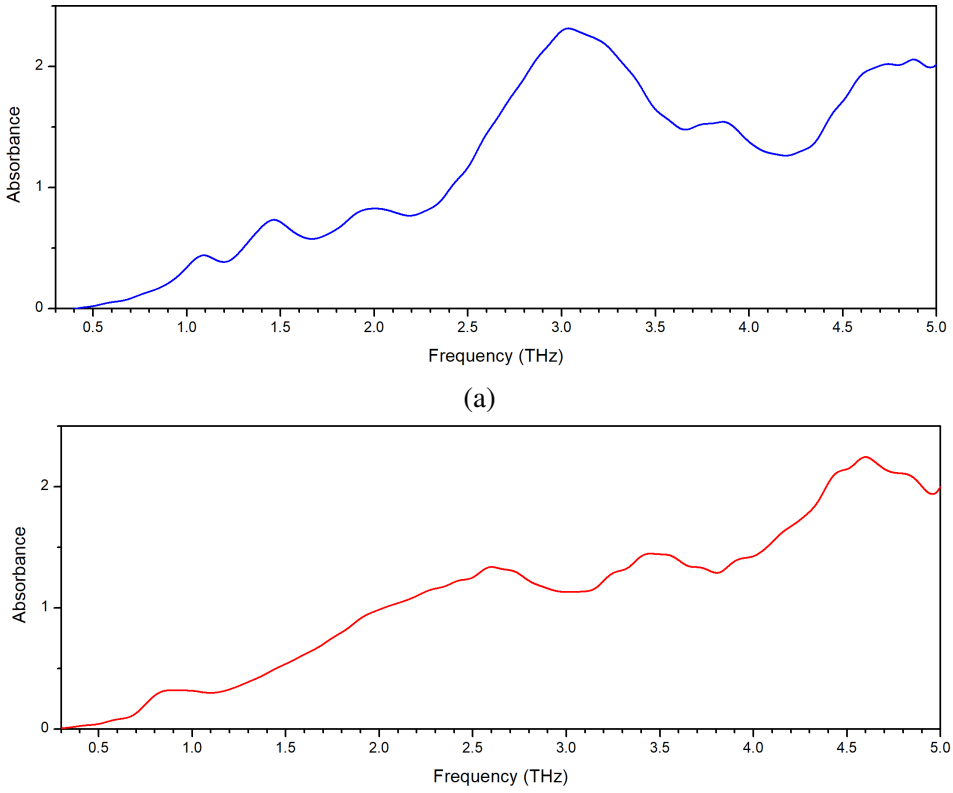

Fig. 3.14 Spectra of Acetamiprid (a) and Metalaxyl (b) from 0.3 to 5THz.

Since the surface of the SRRs produced by MPP had pores, we could not remove the particles of the active substances from the metamaterial. Therefore, we decided to start with

the lowest concentration, 10ppb, and then consequently increase the concentration without cleaning the sample.

We prepared samples diluted in water with concentrations of 0 ppb, 10 ppb, 100 ppb, 10^3 ppb, 10^4 ppb and $5 \cdot 10^4$ ppb of Metalaxyl and 0 ppb, 10 ppb, 100ppb, 10^3 ppb, 10^4 ppb and 10^5 ppb of Acetamiprid. Metalaxyl samples were applied in the 1 THz SRR and Acetamiprid samples were applied both in 0.5 and 1 THz SRRs and were measured after they have dried. We performed measurements at two geometrical configurations, with the SRR gap oriented parallel to the THz polarization and with the gap perpendicular to the polarization. The transmittance measurements of both configurations are presented in Fig. 3.15. The concentrations noted in the figures correspond to the actual number of ppb, for instance after the first measurement of 10ppb we add the 100ppb sample, so the actual concentration is 100ppb plus the remaining residue from earlier meaning 110ppb. The same logic applies to the rest concentrations. We did not detect a notable shift in the resonance as we were aiming. However, if we study the phase difference between the sample's electric field, Φ_S, and the reference's electric field, Φ_R around the resonance region we get some interesting results, that are presented in Fig.3.16. We observe a pattern around the region of the resonance, a shift in the phase difference along two axes. In the first axis, for phase difference equal to zero, we observe a shift in the frequency. In the second axis, that of the resonance frequency, we notice a shift in the phase difference. The data for phase difference equal to zero and for the frequency equal to the resonance in relation to concentration are plotted in Fig. 3.17 and 3.18 respectively. The concentration axis is logarithmic because the samples used mainly differ by one order of magnitude from each other. As we can clearly see, there is a clear linear dependence of the studied quantities to the logarithm of the concentration of the active substance. Moreover, even the lowest concentration of 10 ppb can be identified in all cases.

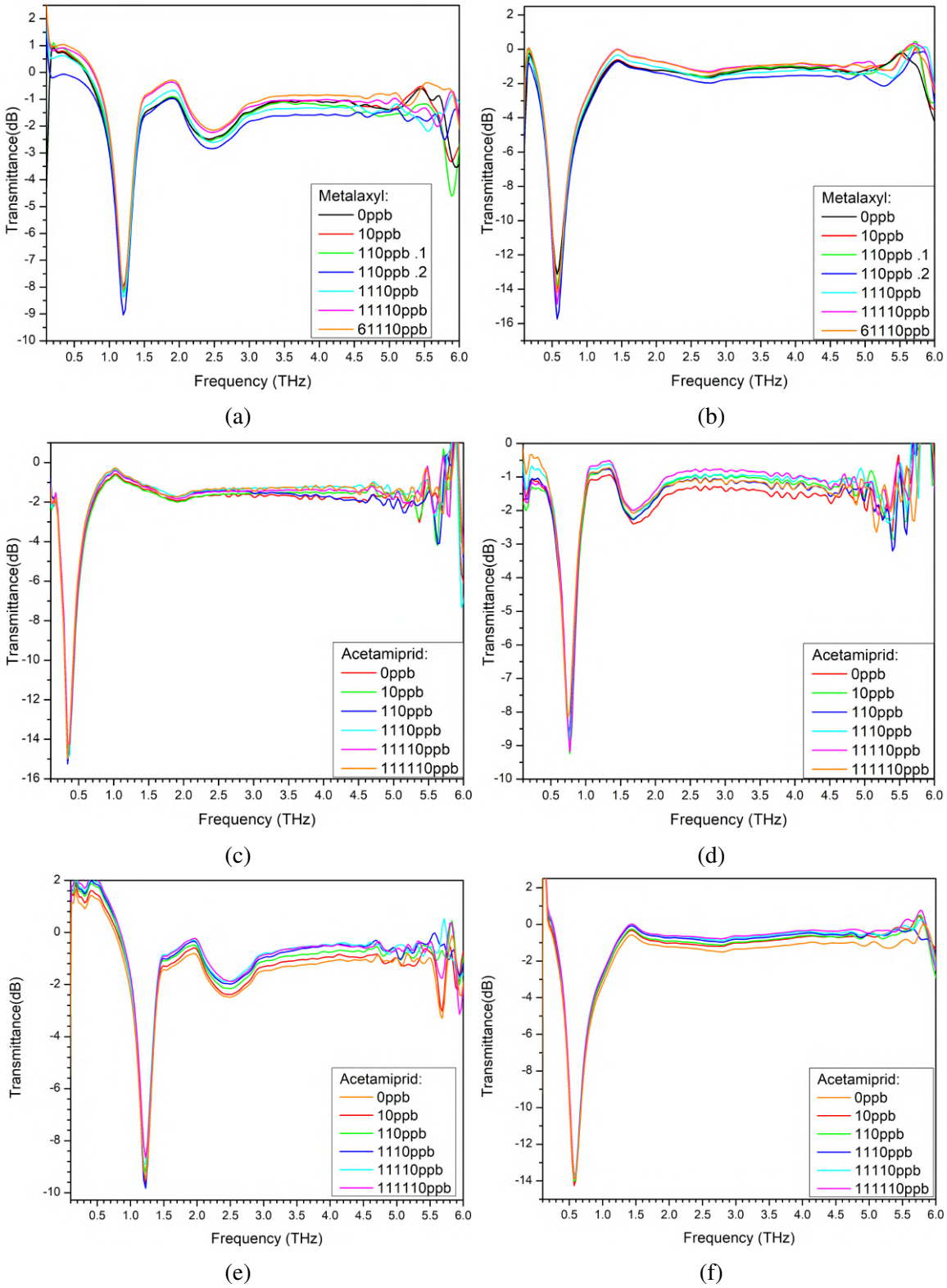

Fig. 3.15 Measured transmittance of Metalaxyl in 1THz SRR (a)(b), of Acetamiprid in 1THz SRR (c)(d) and 0.5THz SRR (e)(f). Polarization in x is in graphs (a)(c)(e) and polarization in y is in (b)(d)(f).

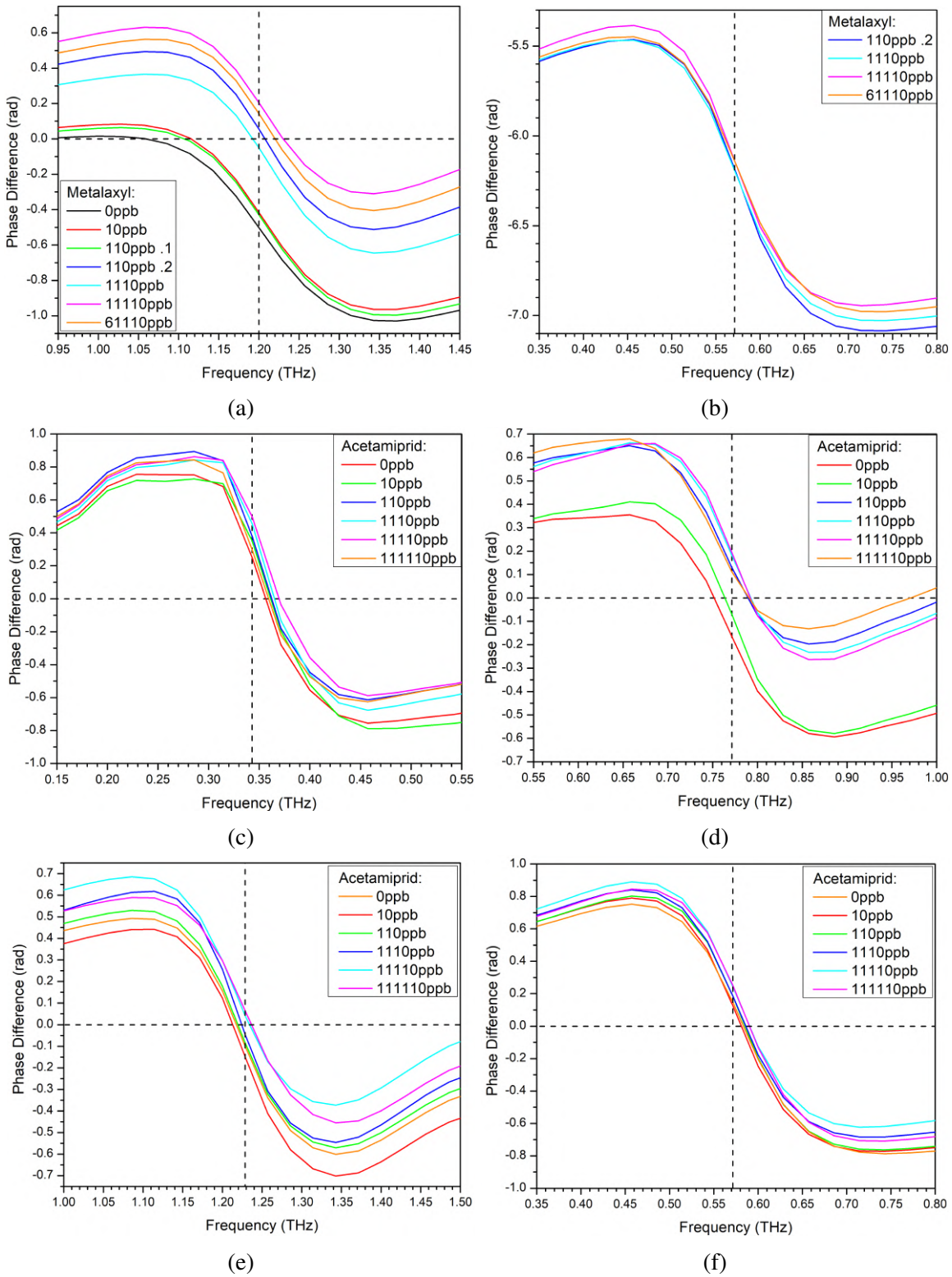

Fig. 3.16 Measured phase difference of Metalaxyl in 1THz SRR (a)(b), of Acetamiprid in 0.5THz SRR (c)(d) and 1THz SRR (e)(f). Polarization in x is in graphs (a)(c)(e) and polarization in y is in (b)(d)(f).

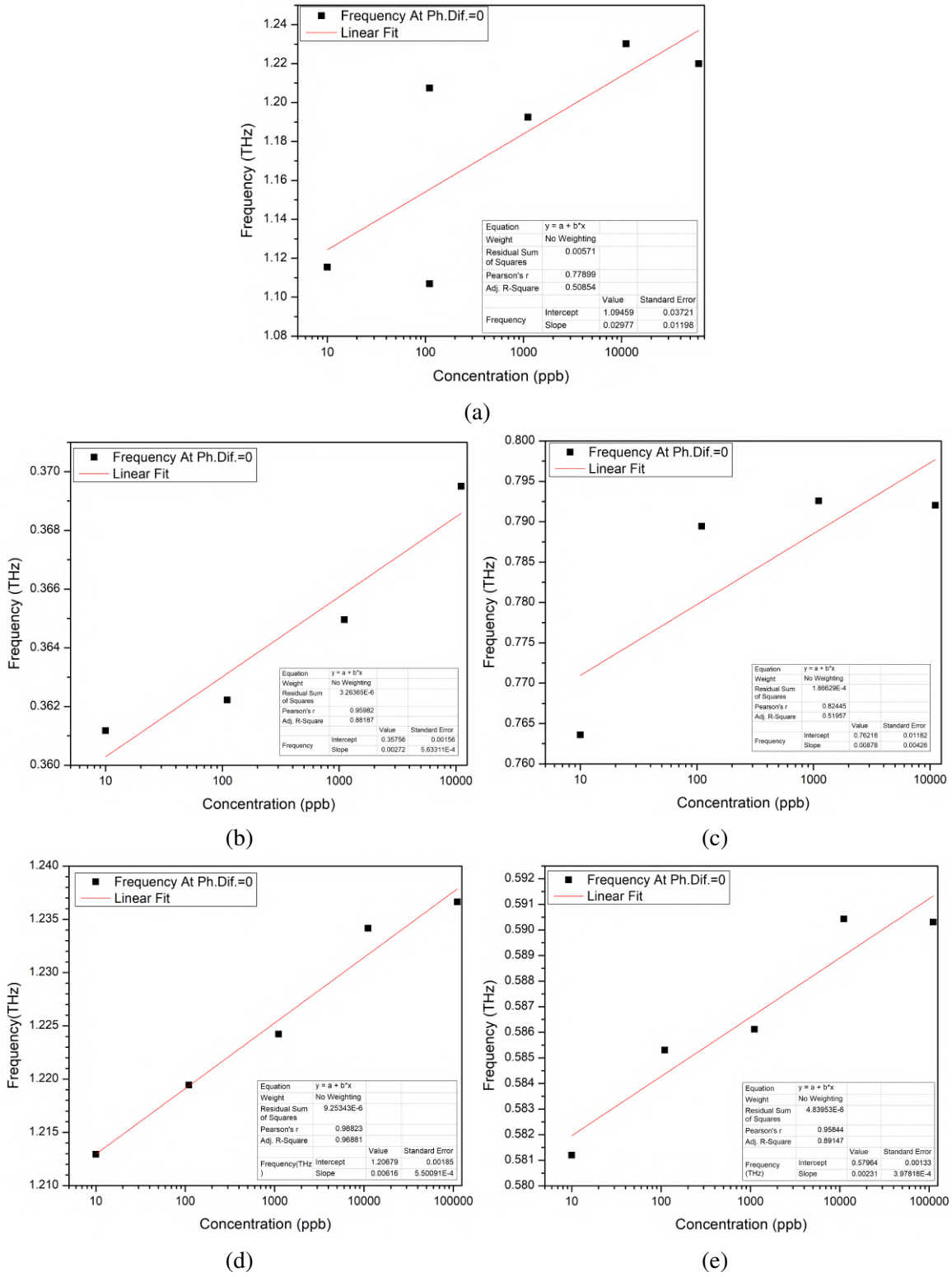

Fig. 3.17 Measured frequency for phase difference equal to zero of Metalaxyl in 1THz SRR (a), of Acetamiprid in 0.5THz SRR (b)(c) and 1THz SRR (d)(e) in relation to concentration. Polarization in x is in graphs (a)(b)(d) and polarization in y is in (c)(e).

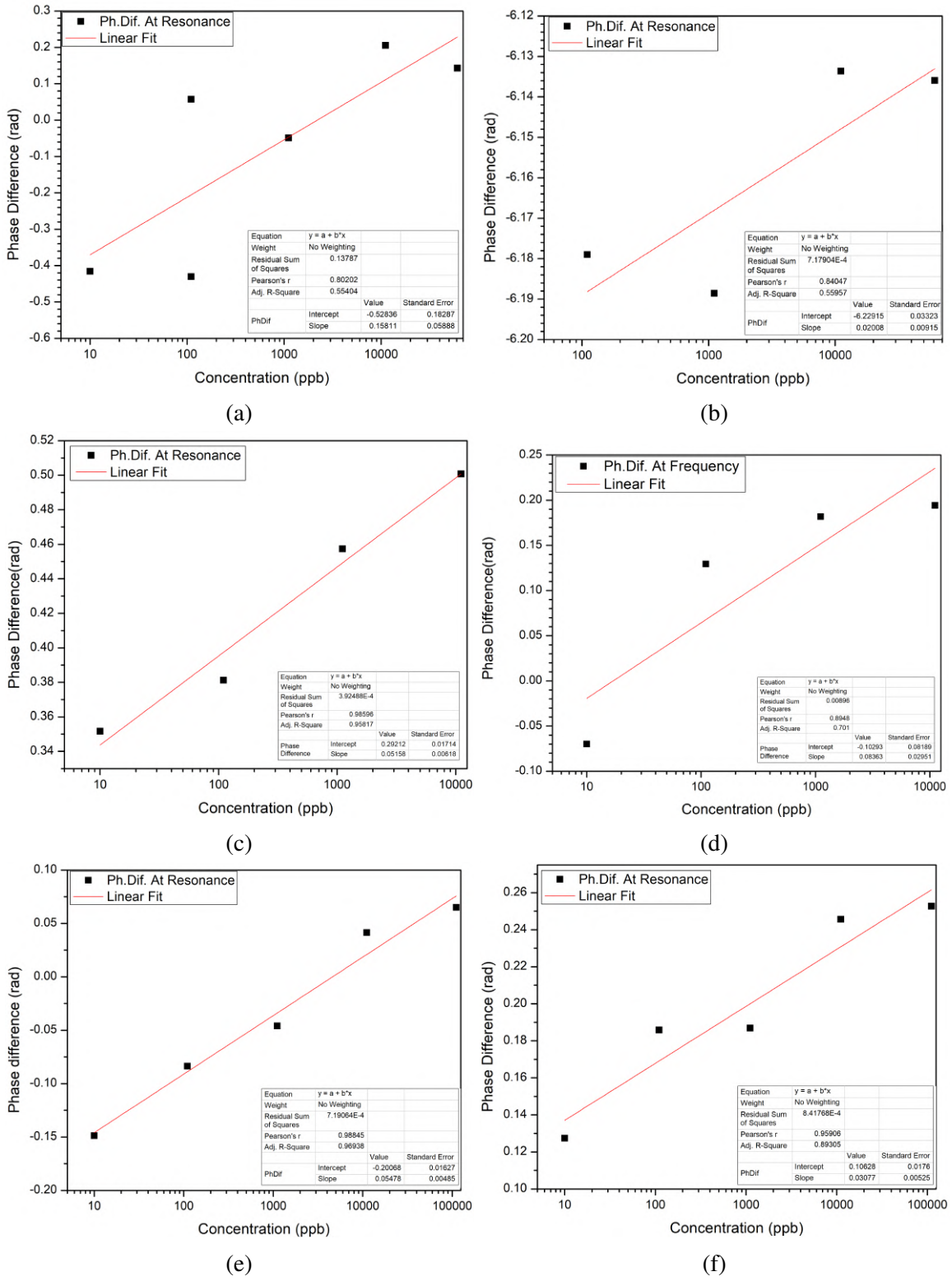

Fig. 3.18 Measured phase difference change for frequency equal to the resonance of Metalaxyl in 1THz SRR (a)(b), of Acetamiprid in 0.5THz SRR (c)(d) and 1THz SRR (e)(f) in relation to concentration. Polarization in x is in graphs (a)(c)(e) and polarization in y is in (b)(d)(f).

Although identifying the lowest possible concentration is of great importance, we would also like to distinguish between different substances. If we plot together the data of Metalaxyl and Acetamiprid at 1 THz from Fig 3.18a and Fig 3.18e

In Fig 3.19a, we used respectively to calculate the shift in the phase difference from the 0ppb concentration.

In Fig 3.19b, we used the data of Metalaxyl and Acetamiprid in the 1THz SRR at x polarization from Fig 3.17a and Fig 3.17d to calculate the shift of the frequency from the frequency at 0ppb concentration.

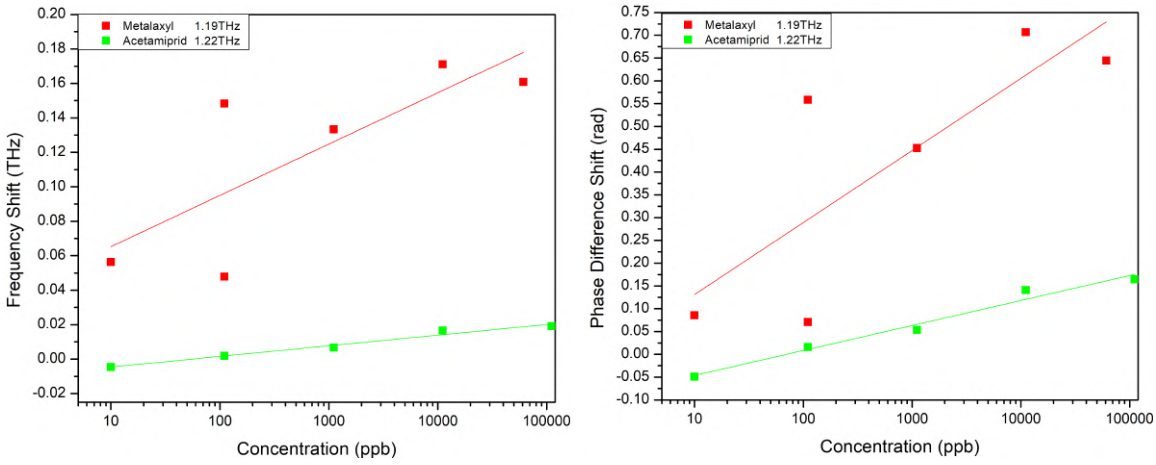

(a) (b)

Fig. 3.19 Phase difference shift of Metalaxyl and Acetamiprid from the 0 ppb concentration (a), Frequency Shift of Metalaxyl and Acetamiprid from the 0 ppb concentration (b). There are also noted the frequencies that each resonance occurs derived from their transmittance spectra.

We can see that the two active substances have different gradients, this technique could also identify the active substance used on the metamaterial.

SRRs and aSRRs made with Babinet's principle

This time we used ethanol to dilute the active substances. We used again Acetamiprid and Metalaxyl as our active substances at the same concentrations as before, meaning 10 ppb to 10^5 ppb. Due to the different construction techniques, the surface does not have any pores, so these metamaterials are washable. After every measurement at a certain concentration, the metamaterial is submerged in ethanol to remove the particles of the active substances.

The Babinet's SRRs were made in the exact same dimensions as the ones made by MPP, this does not mean that they behave the same way. These SRRs did not produce good

resonances and although measurements with active substances were made on them, they will not be presented because no information could be extracted from them.

In the Babinet's aSRRs something went wrong during their construction and the double resonance that the theory predicted is not visible in the experimental data, despite that, measurements with them will be made in the future of this work.

3.3 Conclusions and perspectives

In conclusion, we demonstrated that THz spectroscopy, assisted by metamaterial SRRs, could be used for the detection of pesticides. The enhanced electromagnetic interaction of the THz waves with the active substances on the SRR structures, allowed for the detection of concentrations as low as 10 ppb, a value within the acceptable range implied by the EU regulations. Furthermore, the proposed technique could also differentiate different pesticides from each other, something that attribute to the different molecular weights of the active substances that affect differently the electromagnetic response of the SRRs.

Although our results show a clear trend towards the discrimination of pesticides at concentrations on the few ppb level, there are still plenty of measurements and experimental approaches that need to be performed in order to further validate them. Due to the nature of the fabricated samples that presented a porous surface, cleaning and re-using them was not a feasible and thus further studies are required. For instance, the SRRs based on the Babinet's principle could solve the problem of systematic measurements since these samples consist of metal spattered on a substrate, overcoming the issue of porous surface. Additionally, by designing different resonances within the available THz spectrum, we believe that we will further enhance the ability of the technique to discriminate between different pesticides. Finally, studying the aforementioned samples in the near-field setup that was developed during this thesis, is expected to be an additional, valuable tool that can provide information directly above the region of enhanced interaction of the THz waves with the pesticides.

Chapter 4

Annex

4.1 Fourier Transform Infrared Spectroscopy (FTIR)

Fourier transform infrared spectroscopy or FTIR is a method of obtaining spectra over a wide range of wavelengths. With our FTIR system we can do spectroscopy in the mid-IR and near-IR region.

The near-infrared region covers the area from 10000 to 4000 cm^{-1}, a characteristic of this region is the majority of overtones from C-H, N-H and O-H bonds and combination bands of the fundamental vibrational states[41]. The absorption bands of this region are wide and are easily affected by hydrogen bonding, change in temperature and molecular structures with similar spectra. LED arrays and tungsten lamps are the most usual sources of near-IR [42]. The mid-infrared region stretches from 4000 to 400 cm^{-1} despite the fact that most applications focus only from 4000 to 400 cm^{-1} [43]. This region consists of fundamental vibrational and rotational states of molecules, because of this the absorption bands have stronger signal and are steeper than those in the near-IR. The basic FTIR consists of a broad-band light source and an interferometer. The mirror of the interferometer changes its position, thus changing the central wavelength that reaches the sample. With a Fourier transform we can extrapolate the spectra information from the mirror's path to the wavelength domain.

Our system uses Attenuated Total Reflectance (ATR) as a sampling technique. With this technique infrared radiation reaches an ATR crystal. The radiation experiences total internal reflection several times inside the crystal, as a result evanescent waves traveling at the surface of the crystal are created. The crystal is placed directly under the sample in order to enable the extension of the evanescent waves into the sample, thus gathering more information. The absorption of the evanescent wave is used to measure the absorption spectrum.

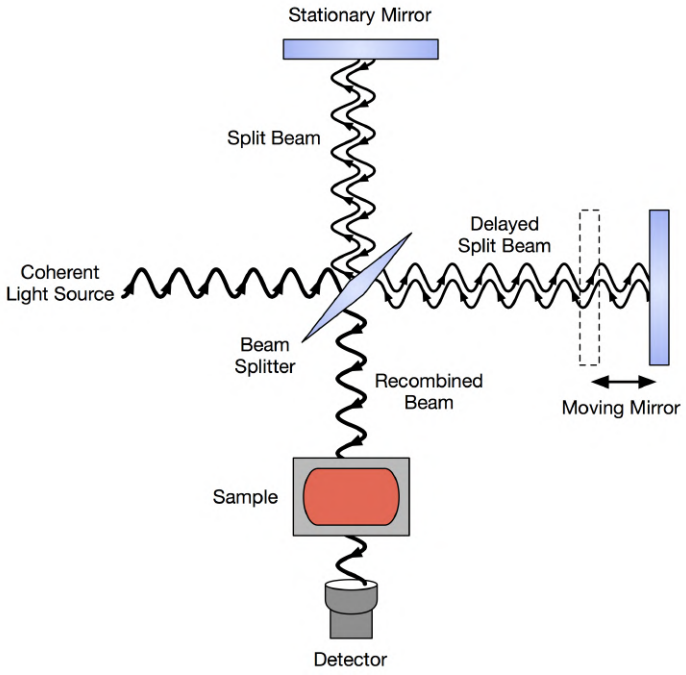

Fig. 4.1 Schematic of a basic FTIR configuration

4.1.1 FTIR results on fruit peels

As a continuation of the previous project, we set out first to find out the minimum detectable concentration of pesticides in fruit peels using the FTIR setup. On dehydrated fruit peels of cucumber and apple, we added on their surface the pesticides Doble and ProfilExtra, one at a time, at different concentrations. We measured the spectra of these surfaces as well as the spectra of water, the pesticides, and the spectra of their active substance.

In Fig 4.2 we present the transmission spectra of Doble of 2.5%, 5%, 12.5%, 25%, 50%, and 100% v/v on cucumber, also the spectra of a plain cucumber, water, Doble and its active substance called Abamectin. We located a region around 1500-750cm^{-1} at which we observe less transmittance due to absorption from Doble and Abamectin. We plotted the minimum transmittance at the previously mentioned region in relation to the concentration of Doble.

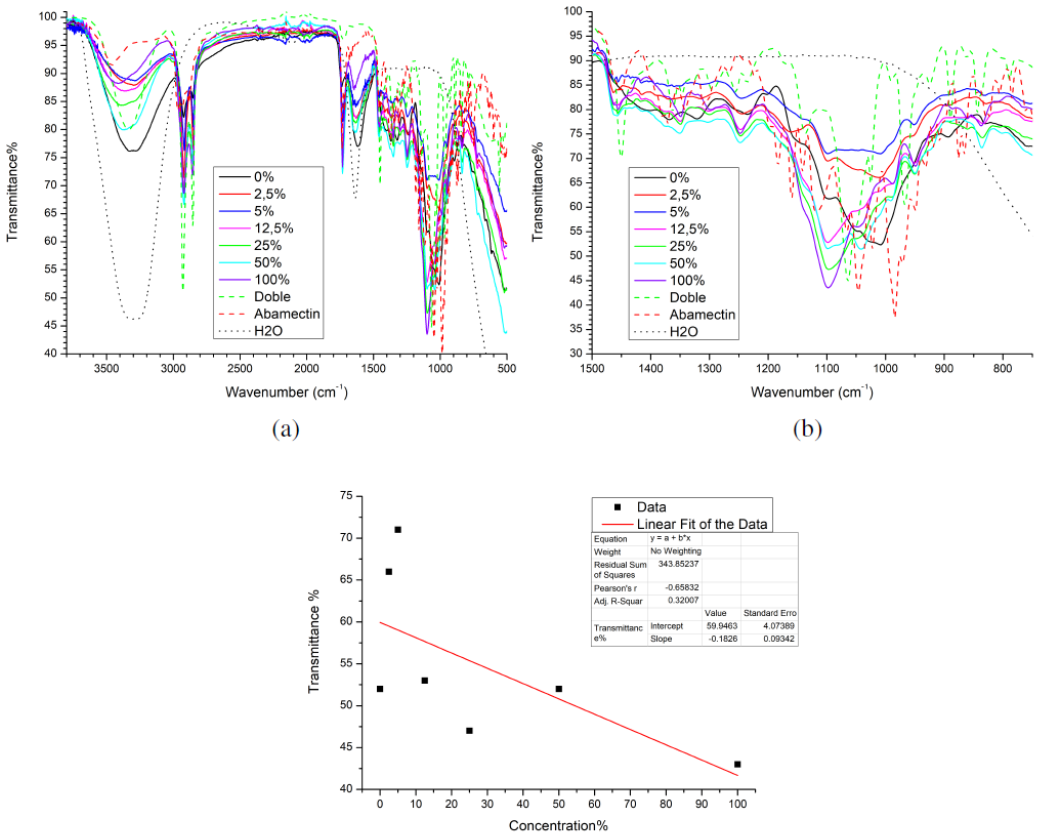

Fig. 4.2 Transmission spectra of cucumber peels, 3850-500cm^{-1} (a), 1500-750cm^{-1} (b) and the minimum transmittance in (b) in relation to concentration (c).

We did the exact same thing with apple peels. In Fig 4.3 are displayed the transmission spectra of ProfilExtra of 2.5%, 5%, 12.5%, 25%, 50% and 100% v/v on apple, also the spectra of water, ProfilExtra and its active substance called Acetamiprid. We located a region around 2300-2100cm^{-1} at which we observe less transmittance due to absorption from ProfilExtra and Acetamiprid and plotted the minimum transmittance in relation to the concentration of ProfilExtra.

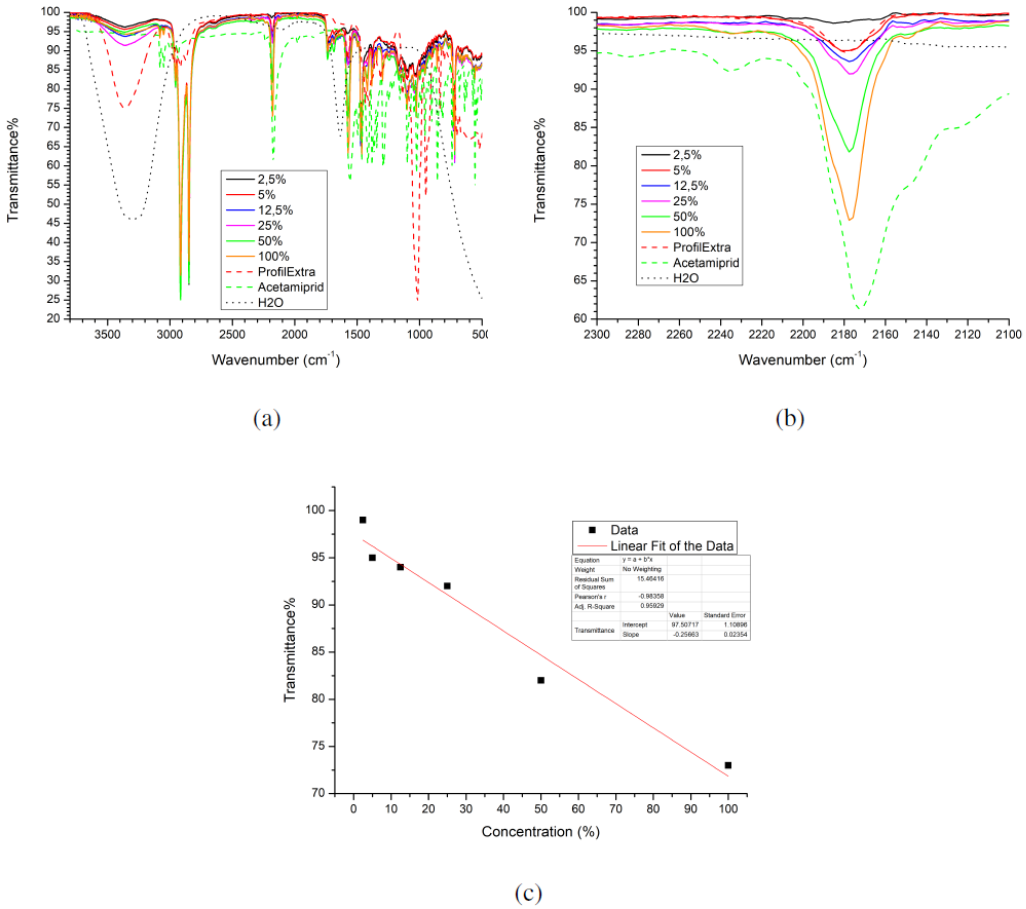

Fig. 4.3 Transmission spectra of apple peels, 3850-500cm^{-1} (a), 2300-2100cm^{-1} (b) and the minimum transmittance in (b) in relation to concentration (c).

We can clearly see the transmittance decreases as the concentration of the pesticides increases, which is to be expected from Beer-Lambert's law [44]. From the measurements on the FTIR, we can see that the lowest concentration we are able to detect with this method is around 2.5%, so we must find a different approach in order to detect even lower concentrations of pesticides.

4.2 Chiral metamaterials

In the duration of this project, measurements for another project were performed that resulted in the submission of a manuscript entitled "Strong and Broadband Pure Optical Activity in 3D Printed THz Chiral Metamaterials". In this project, we measured the response of a chiral metamaterial. Chiral metamaterials have structures that their unit-cell do not have any mirror-symmetry plane. They exhibit optical activity, optical activity is the ability to rotate the polarization of light. In the region of THz radiation, materials with large optical activity cannot be found, so the purpose of the project is the creation of such metamaterial structures.

The structure of the metamaterial is an array of pairs of silver vertical U-shape resonators of twisted arms deposited on to Silicon substrate. The simulations of this structure predict that it possesses large optical activity, due to the rotation of their arms that induces magnetoelectric coupling that causes the chiral's optical activity.

Fig. 4.4 The unit-cell of the chiral structure

The setup used for the measurements is the same one mentioned in section 2.4.1 in transmission mode with a few modifications. The emitter PCA(TX) produces linearly polarized light in the x-axis but this is not absolute, so we use a wire grid polarizer(GP1) at the same axis to reduce any other polarization of light the emitter may produce. After that, the THz pulse reaches the chiral metamaterial. Then, the transmitted wave passes through another wire-grid polarizer(GP2) of tuneable direction. Finally, the wave is detected by the receiver(RX), positioned in a 45^0 angle in relation to the x-axis, in order to detect equally both in the x-axis and in the y-axis.

In Fig 4.6 follow the measurements accompanied with the simulation results of the second wire-grid polarizer(GP2) at 0^0 and 90^0.
The experimental results are in good agreement with the theoretical data. The experimental results show optical activity up to 25^0 for 1THz with an unmatched bandwidth and with a few

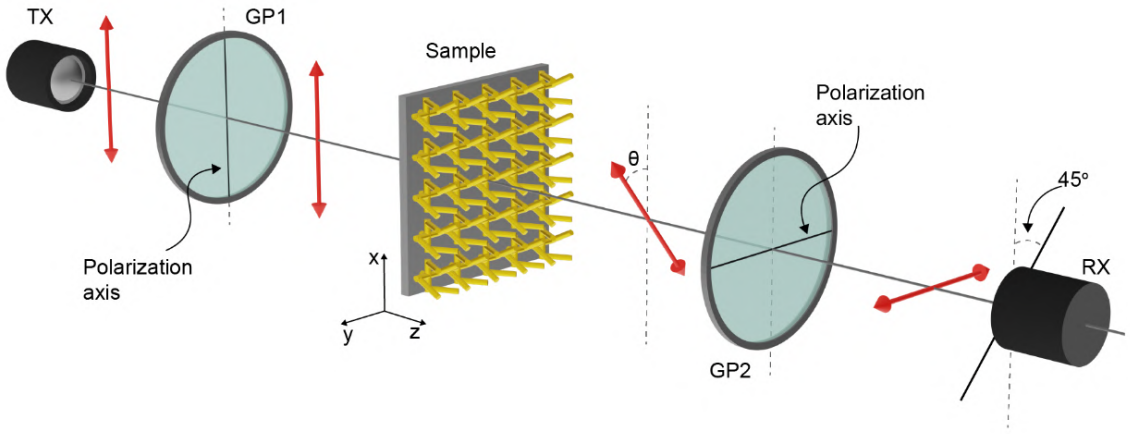

Fig. 4.5 Schematic of the setup used to measure the chiral metamaterial's response.

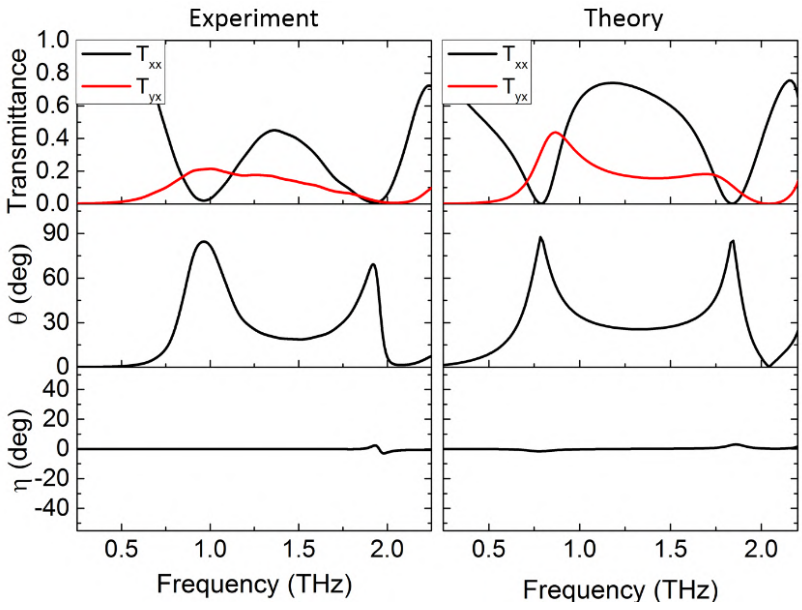

Fig. 4.6 Transmittance measurements of the chiral metamaterial for the position of GP2 at 0^0 and 90^0 (top), optical activity , $\theta(middle)$, and ellipticity , $\eta(bottom)$. The experimental measurements are presented on the left while the theoretical ones on the right.

modifications from the theoretical optimizations it could reach 45^0. Although different from the general project, chiral metamaterials could also be used as a pesticide detector like the SRRs we use, but instead of a frequency shift we would detect a shift in the optical activity of the metamaterial.

4.3 Near - field Imaging

The near – field imaging system enables us to scan samples with maximum accuracy of 50um under the correct conditions.

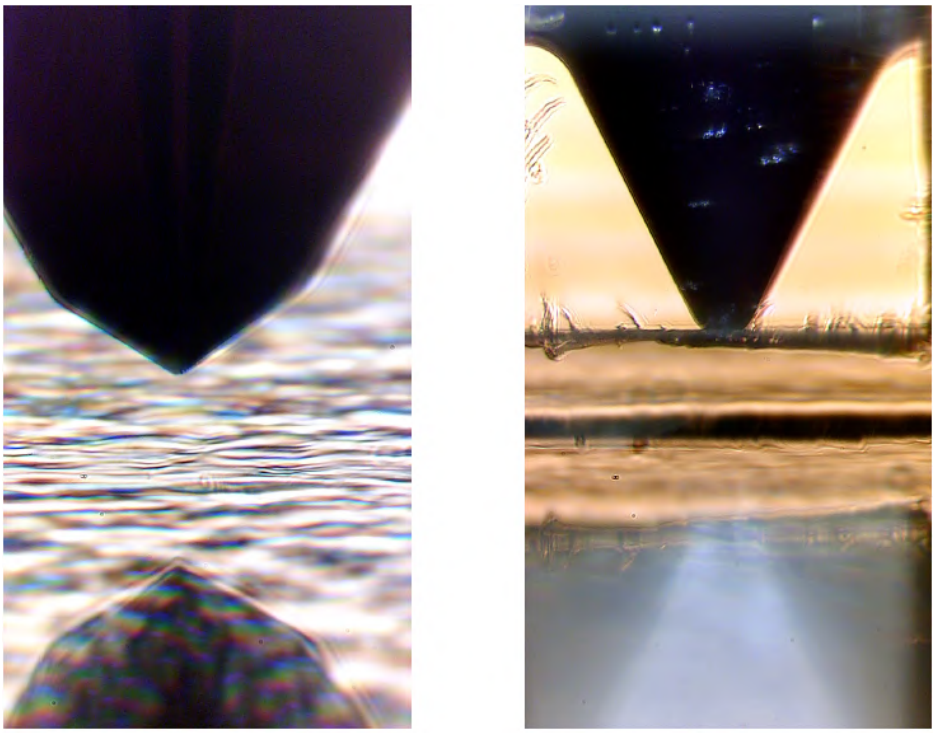

(a) (b)

Fig. 4.7 Images of two different micro-probes by the second imaging system.

4.3.1 Calibration

To scan a sample, we must first calibrate the program responsible for the recording of the THz field, the calibration would not be possible without the use of the two imaging systems mentioned previously in 2.4.2. The procedure starts by placing an object of relatively small dimensions, like the tip of a needle or cone structures, at the mechanical stage. We move the object under the microscope objective and we save its position, then we move it under the THz micro-probe where with the use of the second imaging system we align the object with the micro-probe. This alignment is done by bringing the object into focus and saving again its position, we are aware that it is not the most accurate method due to the fact that the depth of field of the camera gives us an error but this imaging system is placed roughly at 45 degrees from the x axis of the stage so this the only way for the alignment. The program calculates

the difference in the distance between the two positions, now we can easily place a sample under the THz micro-probe by simply adding the calculated distance to its position under the microscope's lens. We can repeat the process with the use of a smaller object in order to improve the accuracy of our calibration. After completing the calibration, we perform raster scanning on the sample in order to record an image of it in the THz domain. The dimensions of the scan and the step it uses are controlled by the same program as the calibration.

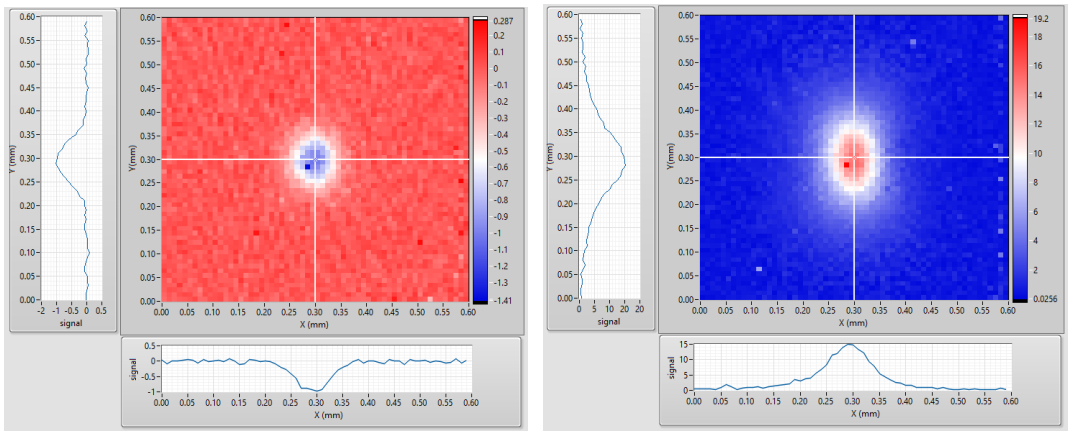

(a) (b)

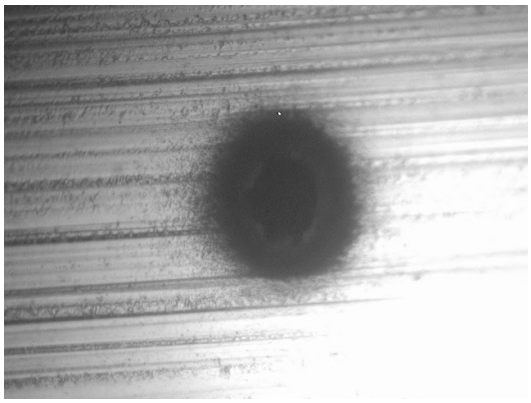

(c)

Fig. 4.8 Image in the THz domain of a 50μm pinhole at 1480.4ps (a) and at 0.3THz (b), and the image of the pinhole in the microscope(c). The signal of the cross-section is also included.

4.3.2 Lighting

The lighting of both optical systems is crucial for the near – field system. The first imaging system, in which we observe the surface of the sample is placed in plane perpendicular to the sample. White light is directed by a mirror on a beamsplitter, the reflected light passes

through the microscope's lens and is focused on the sample. It gets reflected from the sample, passes through the microscope's lens again, through the same beamsplitter and then reaches the camera.

The second imaging system is responsible for the imaging of the THz micro-probe and the surface, without it we would not be able neither to calculate the distance of the sample from the probe nor calibrate the program required for the THz imaging. This imaging system is in the same plane as the sample, the lighting is placed behind the THz micro-probe directed to the camera.

4.3.3 Resolution

The THz micro-probe we use for the measurements has spectral range from 0.1 to 1.5THz and spatial resolution of 20um. The resolution of the imaging system is also influenced by the distance the probe has from the sample, so in order to achieve maximum resolution we must place the probe at least 20um above the sample's surface. We scanned various samples, presented in Fig4.8, Fig4.9 and Fig4.10 in order to calculate the resolution of the system, some of those samples are a pinhole of 50um in diameter, a diffraction grating and a square silicon structure.

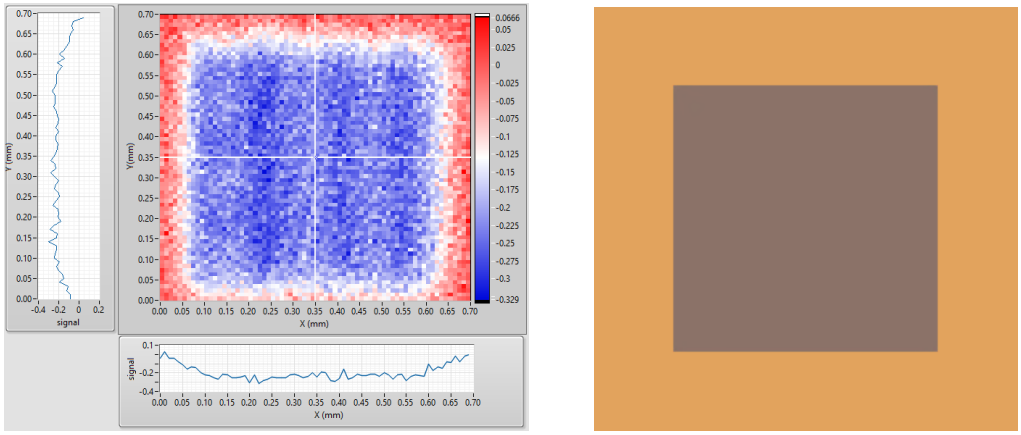

(a) (b)

Fig. 4.9 Image in the THz domain of a 500μm Silicon square(a) and its image in the microscope(b). The signal of the cross-section is also included.

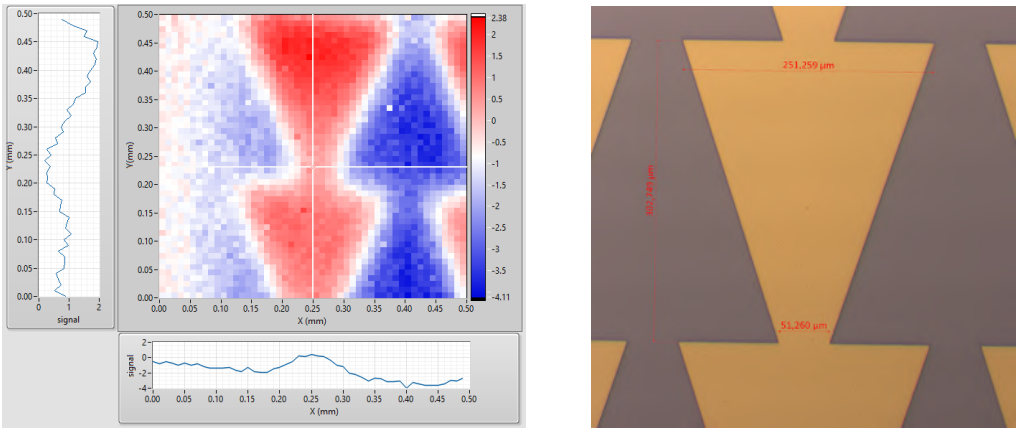

(a) (b)

Fig. 4.10 Image in the THz domain of diffraction gratings(a) and their image in the microscope(b). The signal of the cross-section is also included.

From the signals of the cross-section, we can calculate the resolution of the image by measuring the size of the slopes between two plateaus of the signal and dividing it by two.

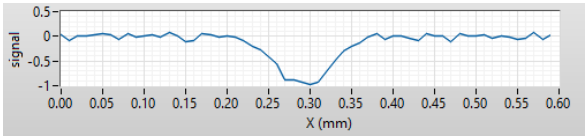

Fig. 4.11 Signal of the cross-section of the pinhole at 1480.4 ps.

For example, we take the signal of the cross-section of the pinhole at 1480.4ps from Fig 4.11, the slope between the two plateaus in the signal is from 0.31mm to 0.37mm so the resolution of this image is $30\mu m$. From the rest of the images, we calculate that the Si square has a resolution of $50\mu m$ and the diffraction gratings have a resolution of $25\mu m$ [45]. The diffraction gratings have a better resolution because the distance between the sample and the micro-probe was smaller than the rest of the samples.

References

[1] Gwyn P Williams. Filling the THz gap—high power sources and applications. *Reports on Progress in Physics*, 69(2):301–326, February 2006.

[2] Ch. Fattinger and D. Grischkowsky. Terahertz beams. *Applied Physics Letters*, 54(6):490–492, February 1989. Publisher: American Institute of Physics.

[3] Gillian C. Walker, Elizabeth Berry, Nick N. Zinov'ev, Anthony J. Fitzgerald, Robert E. Miles, J. Martyn Chamberlain, and Michael A. Smith. Terahertz imaging and international safety guidelines. 4682:683–690, May 2002. Conference Name: Medical Imaging 2002: Physics of Medical Imaging ADS Bibcode: 2002SPIE.4682..683W.

[4] Xi-Cheng Zhang and Jingzhou Xu. *Introduction to THz Wave Photonics*. Springer US, Boston, MA, 2010.

[5] Calvin Yu, Shuting Fan, Yiwen Sun, and Emma Pickwell-Macpherson. The potential of terahertz imaging for cancer diagnosis: A review of investigations to date. *Quantitative Imaging in Medicine and Surgery*, 2(1):33–45, March 2012.

[6] Nagendra Paradad Yadav, Guo-Zhen Hu, Zheng-Peng Yao, and Ashish Kumar. Diagnosis of dental problem by using terahertz technology. *Journal of Electronic Science and Technology*, 19(3):100082, September 2021.

[7] Journal of Infrared, Millimeter, and Terahertz Waves.

[8] Terahertz radiation and the skin: a review.

[9] Alexander I. McIntosh, Bin Yang, Stephen M. Goldup, Michael Watkinson, and Robert S. Donnan. Terahertz spectroscopy: a powerful new tool for the chemical sciences? *Chemical Society Reviews*, 41(6):2072–2082, February 2012. Publisher: The Royal Society of Chemistry.

[10] Olga P. Cherkasova, Danil S. Serdyukov, Eugenia F. Nemova, Alexander S. Ratushnyak, Anna S. Kucheryavenko, Irina N. Dolganova, Guofu Xu, Maksim Skorobogatiy, Igor V. Reshetov, Peter S. Timashev, Igor E. Spektor, Kirill I. Zaytsev, and Valery V. Tuchin. Cellular effects of terahertz waves. *Journal of Biomedical Optics*, 26(9):090902, September 2021.

[11] J. Axel Zeitler, Philip F. Taday, David A. Newnham, Michael Pepper, Keith C. Gordon, and Thomas Rades. Terahertz pulsed spectroscopy and imaging in the pharmaceutical setting–a review. *The Journal of Pharmacy and Pharmacology*, 59(2):209–223, February 2007.

[12] Philip F. Taday. Applications of terahertz spectroscopy to pharmaceutical sciences. *Philosophical Transactions. Series A, Mathematical, Physical, and Engineering Sciences*, 362(1815):351–363; discussion 363–364, February 2004.

[13] Fei Shen and Yi-Bin Ying. [Applications of terahertz spectroscopy and imaging techniques in food safety inspection]. *Guang Pu Xue Yu Guang Pu Fen Xi = Guang Pu*, 29(6):1445–1449, June 2009.

[14] Aifeng Ren, Adnan Zahid, Xiaodong Yang, Akram Alomainy, Muhammad Imran, and Qammer Abbasi. Terahertz (THz) application in food contamination detection. December 2019.

[15] Xiaojian Fu, Yujie Liu, Qi Chen, Yuan Fu, and Tie Jun Cui. Applications of Terahertz Spectroscopy in the Detection and Recognition of Substances. *Frontiers in Physics*, 10, 2022.

[16] Yu Heng Tao, Anthony J. Fitzgerald, and Vincent P. Wallace. Non-Contact, Non-Destructive Testing in Various Industrial Sectors with Terahertz Technology. *Sensors*, 20(3):712, January 2020. Number: 3 Publisher: Multidisciplinary Digital Publishing Institute.

[17] The 2017 terahertz science and technology roadmap - IOPscience.

[18] P.u. Jepsen, D.g. Cooke, and M. Koch. Terahertz spectroscopy and imaging – Modern techniques and applications. *Laser & Photonics Reviews*, 5(1):124–166, 2011. _eprint: https://onlinelibrary.wiley.com/doi/pdf/10.1002/lpor.201000011.

[19] Kaori Fukunaga, Yuichi Ogawa, Shin'ichiro Hayashi, and Iwao Hosako. Terahertz spectroscopy for art conservation. *IEICE Electronics Express*, 4(8):258–263, 2007.

[20] Antonino Cosentino. Terahertz and Cultural Heritage Science: Examination of Art and Archaeology. *Technologies*, 4(1):6, March 2016. Number: 1 Publisher: Multidisciplinary Digital Publishing Institute.

[21] Sergio Ioppolo, Marco A. Allodi, Brett A. McGuire, Matthew J. Kelley, and Geoffrey A. Blake. *Terahertz Time Domain Spectroscopy of Simple Astrophysically Relevant Ices: the Structure of the Ice*. June 2013. Conference Name: 68th International Symposium on Molecular Spectroscopy Pages: ETE05 ADS Bibcode: 2013mss..confETE05I.

[22] Satoki Matsushita, Keiichi Asada, Ray Blundell, Chih-Cheng Chang, Ming-Tang Chen, Paul Grimes, Johnson Han, Hiroyuki Hirashita, Paul T. P. Ho, Ted Huang, Makoto Inoue, Homin Jiang, Patrick Koch, Derek Kubo, Pierre Martin-Cocher, Zheng Meyer-Zhao, Masanori Nakamura, Hiroaki Nishioka, George Nystrom, Scott Paine, Nimesh Patel, Hung-Yi Pu, Philippe Raffin, William Snow, and Ranjani Srinivasan. Greenland Telescope: Imaging Black Hole Shadow and THz Astronomy. 29:2251138, August 2015. Conference Name: IAU General Assembly ADS Bibcode: 2015IAUGA..2251138M.

[23] John F. Federici, Brian Schulkin, Feng Huang, Dale Gary, Robert Barat, Filipe Oliveira, and David Zimdars. THz imaging and sensing for security applications—explosives, weapons and drugs. *Semiconductor Science and Technology*, 20(7):S266, June 2005.

[24] Magnetism from conductors and enhanced nonlinear phenomena. *IEEE Transactions on Microwave Theory and Techniques*, 47(11):2075–2084, November 1999. Publisher: IEEE.

[25] Experimental Verification of a Negative Index of Refraction | Science.

[26] Wei Ming Zhu, Ai Qun Liu, Xu Ming Zhang, Din Ping Tsai, Tarik Bourouina, Jing Hua Teng, Xin Hai Zhang, Hong Chen Guo, Hendrix Tanoto, Ting Mei, Guo Qiang Lo, and Dim Lee Kwong. Switchable Magnetic Metamaterials Using Micromachining Processes. *Advanced Materials*, 23(15):1792–1796, April 2011.

[27] Na Liu, Hongcang Guo, Liwei Fu, Stefan Kaiser, Heinz Schweizer, and Harald Giessen. Three-dimensional photonic metamaterials at optical frequencies. *Nature Materials*, 7(1):31–37, January 2008.

[28] Jason Valentine, Shuang Zhang, Thomas Zentgraf, Erick Ulin-Avila, Dentcho A. Genov, Guy Bartal, and Xiang Zhang. Demonstration of Negative Refractive Index in a Three Dimensional Optical Metamaterial. In *Conference on Lasers and Electro-Optics/Quantum Electronics and Laser Science Conference and Photonic Applications Systems Technologies (2008), paper QPDB2*, page QPDB2. Optica Publishing Group, May 2008.

[29] Tie Jun Cui, David Smith, and Ruopeng Liu, editors. *Metamaterials: Theory, Design, and Applications*. Springer US, Boston, MA, 2010.

[30] Dong-Kyu Lee, Giyoung Kim, Chulki Kim, Young Min Jhon, Jae Hun Kim, Taikjin Lee, Joo-Hiuk Son, and Minah Seo. Ultrasensitive Detection of Residual Pesticides Using THz Near-Field Enhancement. *IEEE Transactions on Terahertz Science and Technology*, 6(3):389–395, May 2016.

[31] Zhuoyi Chen, Fangfang Qu, Yue Wang, and Pengcheng Nie. Terahertz dual-band metamaterial absorber for trace indole-3-acetic acid and tricyclazole molecular detection based on spectral response analysis. *Spectrochimica Acta Part A: Molecular and Biomolecular Spectroscopy*, 263:120222, December 2021.

[32] Fangfang Qu, Lei Lin, Zhuoyi Chen, Alwaseela Abdalla, and Pengcheng Nie. A terahertz multi-band metamaterial absorber and its synthetic evaluation method based on multivariate resonant response fusion for trace pesticide detection. *Sensors and Actuators B: Chemical*, 336:129726, June 2021.

[33] Nathan M. Burford and Magda O. El-Shenawee. Review of terahertz photoconductive antenna technology. *Optical Engineering*, 56, 2017.

[34] Paul C Gow. Schottky Enhanced Photo-Dember Terahertz Emitters.

[35] Dima Fishman. THz Time-Domain Spectroscopy For Dummies.

[36] Electromagnetic Radiation: Field Memo | Occupational Safety and Health Administration.

[37] Constantine A. Balanis. *Antenna theory: analysis and design*. John Wiley, Hoboken, NJ, 3rd ed edition, 2005.

[38] Ultrafast laser nanostructuring of photopolymers: A decade of advances | Elsevier Enhanced Reader.

[39] Andrey I. Aristov, Maria Manousidaki, Artem Danilov, Konstantina Terzaki, Costas Fotakis, Maria Farsari, and Andrei V. Kabashin. 3D plasmonic crystal metamaterials for ultra-sensitive biosensing. *Scientific Reports*, 6(1):25380, May 2016.

[40] Xiangxiang Cheng and Chonghua Fang. Metamaterial design applying Babinet's principle. In *2014 XXXIth URSI General Assembly and Scientific Symposium (URSI GASS)*, pages 1–4, August 2014.

[41] Da-Wen Sun. *Infrared spectroscopy for food quality analysis and control*. Academic Press, Burlington, MA, 1st ed edition, 2009.

[42] Ine L. Jernelv, Karolina Milenko, Silje S. Fuglerud, Dag Roar Hjelme, Reinold Ellingsen, and Astrid Aksnes. A review of optical methods for continuous glucose monitoring. *Applied Spectroscopy Reviews*, 54(7):543–572, August 2019.

[43] David I. Ellis and Royston Goodacre. Metabolic fingerprinting in disease diagnosis: biomedical applications of infrared and Raman spectroscopy. *Analyst*, 131(8):875–885, 2006. Publisher: The Royal Society of Chemistry.

[44] Victor Gold, editor. *The IUPAC Compendium of Chemical Terminology: The Gold Book*. International Union of Pure and Applied Chemistry (IUPAC), Research Triangle Park, NC, 4 edition, 2019.

[45] Jens Neu and Charles A. Schmuttenmaer. Tutorial: An introduction to terahertz time domain spectroscopy (THz-TDS). *Journal of Applied Physics*, 124(23):231101, December 2018.